Single cell biochemistry to visualize antigen presentation and drug resistance

Griekspoor, A.C.

Spatial Separation of HLA-DM/HLA-DR Interactions within MIIC and Phagosome-Induced Immune Escape

Reprinted from Immunity, vol. 22: 221–233,

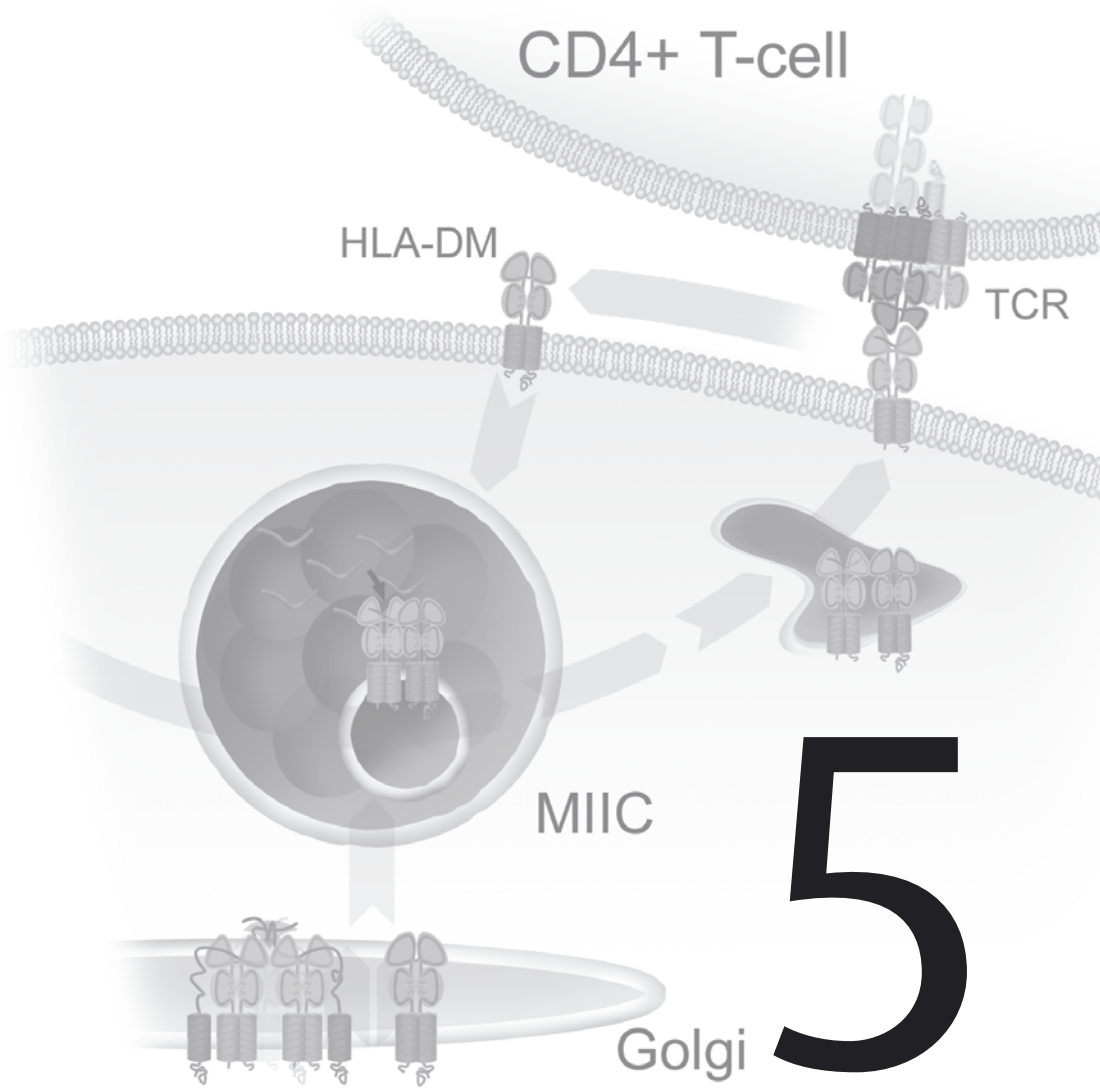

5

Spatial Separation of HLA-DM/HLA-DR Interactions within MIIC and Phagosome-Induced Immune Escape

Alexander Griekspoor*[1], Wilbert Zwart*[1], Coenraad Kuijl[1], Marije Marsman[1], Jacco van Rheenen[2‡], Hans Janssen[2], Jero Calafat[2], Marieke van Ham[1§], Lennert Janssen[1], Marcel van Lith[1¶], Kees Jalink[2], and Jacques Neefjes[1]

[1] Division of Tumour Biology, The Netherlands Cancer Institute, Amsterdam, The Netherlands.
[2] Division of Cell Biology, The Netherlands Cancer Institute, Amsterdam, The Netherlands.

Major Histocompatibility Complex (MHC) class II molecules, including Human Leukocyte Antigen (HLA)-DR, present peptide fragments from proteins degraded in the endocytic pathway. HLA-DR is targeted to late-endocytic structures named MHC class II-containing Compartments (MIIC), where it interacts with HLA-DM. This chaperone stabilizes HLA-DR during peptide exchange and is critical for successful peptide loading. To follow this process in living cells, we have generated cells containing HLA-DR3/Cyan Fluorescent Protein (CFP), HLA-DM/Yellow Fluorescent Protein (YFP), and invariant chain. HLA-DR/DM interactions were observed by Fluorescence Resonance Energy Transfer (FRET). These interactions were pH insensitive, yet occurred only in internal structures and not at the limiting membrane of MIIC. In a cellular model of infection, phagosomes formed a limiting membrane surrounding internalized Salmonella. HLA-DR and HLA-DM did not interact in Salmonella-induced vacuoles, and HLA-DR was not loaded with antigens. The absence of HLA-DR/DM interactions at the limiting membrane prevents local loading of MHC class II molecules in phagosomes. This may allow these bacteria to successfully evade the immune system.

CORRESPONDENCE
Jacques J. Neefjes
Division of Tumour Biology
The Netherlands Cancer Institute
Plesmanlaan 121
1066 CX Amsterdam
The Netherlands
Tel.: +31 20 512 2012
Fax: +31 20 512 2029
E-mail: j.neefjes@nki.nl

Immunity 2005
Vol. 22: 221-233

Introduction

Major Histocompatibility Complex (MHC) class II molecules present peptide fragments of antigens degraded in the endocytic pathway to $CD4^+$ T cells (1). This is a prerequisite for efficient antibody responses and the establishment of an effective immunological memory. In order to contact antigens, MHC class II molecules like Human Leukocyte Antigen (HLA)-DR (DR) are chaperoned from the endoplasmic reticulum (ER) to late endocytic structures (called MHC class II containing compartments, or MIIC (2)) by the invariant chain. Here, the invariant chain is degraded except for a small fragment called CLIP, which remains in the peptide binding groove of DR (3). HLA-DM (DM), a second dedicated chaperone, is required to stabilize the "empty" MHC class II molecules and supports the exchange of both CLIP and low-affinity peptides for a peptide with high affinity (4-6) that fills pocket 1 in the peptide binding groove (7). The direct interaction between DM and DR has been shown in *in vitro* reconstitution experiments and coisolations. This interaction was pH sensitive and of low af-

* A. Griekspoor and W. Zwart contributed equally to this paper; Present addresses: ‡ Albert Einstein College of Medicine, New York, NY, USA; § Sanquin Research at CLB, Amsterdam, The Netherlands; ¶ University of Durham, Durham, UK

finity (8, 9). DM interacts with a lateral site on DR via hydrophobic surfaces, but the exact factors that contribute to this process remain unclear (10-12). More recently, a nonpolymorphic MHC class II homolog has been identified, called HLA-DO (DO). DO stably interacts with DM, reducing its chaperoning activity on DR in a pH-dependent manner (13-15). Like the DR/DM complex, the DM/DO complex is targeted to the MIIC.

MIIC are characterized by a multilamellar and/or multivesicular structure. Multivesicular bodies (MVB) can be converted into multilamellar structures by changes in protein content (16) and both type of structures most likely reflect different maturation states (17). The internal structures differ from the limiting membrane by both protein and lipid composition. Whereas DR and DM can be found in both domains, other late-endocytic proteins like tetraspans, and lipids like cholesterol and lyso-bis-PA, are usually located at the internal structures (18, 19). Although tetraspans like CD63 and CD82 interact with DM or DR (20, 21), the functional consequences are unclear. Still, internal structures differ in composition from the limiting membrane, and this may affect the interaction between DR and its chaperone DM and ultimately antigen presentation (22). The failure to visualize these interactions due to the limited resolution of light microscopy prevented any conclusion about spatial specialization within MIIC.

The formation of internal structures that characterize the morphology of a MVB is the result of a complicated series of events. It requires the activities of a PI3-kinase hVPS34, ESCRT complexes, ubiquitination, and acidification (23). Inhibition of hVPS34 or acidification results in expanded late-endosomal structures without internal vesicles (24). Such treatments also affect the MIIC and inhibit antigen presentation by MHC class II molecules (25, 26). Pathogens like *Salmonella typhimurium*, *Mycobacterium tuberculosis*, and *Mycobacterium leprae* survive in phagosomes (27, 28), structures composed of only a limiting membrane surrounding the bacteria. These intracellular bacteria have been reported to reduce or even eliminate antigen presentation by MHC class II molecules (29-31), but the underlying mechanism remains elusive.

Here, we studied the interaction between DM and DR3 in living cells by Fluorescence Resonance Energy Transfer (FRET). Applying Confocal Laser-Scanning Microscopy (CLSM)-FRET microscopy allowed us to visualize these interactions at unprecedented resolution within MIIC of living cells. This interaction was not affected by neutralization of pH, and it occurred exclusively in the internal structures of MIIC. No interaction was observed in MIIC devoid of internal structures after long-term chloroquine treatment or knockdown of hVPS34. Similarly, phagosomes in which many intracellular pathogens survive often lack internal membranes. This can occur when hVPS34 is inactivated (32), or when a downstream product of hVPS34 (PI(3,5)P2) is hydrolyzed by the *Salmonella*-secreted PIP2-phosphatase SopB (33). We show that at the limiting membrane of a *Salmonella*-induced phagosome (SCV) DM failed to interact with DR3, again using FRET. Consequently, DR3 was not loaded with antigens within the SCV while antigen loading within multivesicular MIIC continued in the infected cells. Local MHC class II-restricted immune escape of intracellular pathogens like *Salmonella* appears to be a consequence of subvesicular structural differences within the MIIC, where HLA-DM interacts with HLA-DR in MHC class II loading microdomains in the internal structures, but not at the limiting membrane.

Experimental Procedures

Antibodies and fluorophores

The following antibodies were used. Mouse monoclonal antibodies HC-10 (class I Heavy Chain) (34); anti-CD63 (NKI-C3) (35); HLA-DR–specific mAbs 1B5 (36) and Tü36 (37), and the HLA-DMα-specific mAb 5C1 (8). Rabbit polyclonal sera anti-DR (38), anti-GFP, anti-*Salmonella* (*Salmonella* 30kD) and rabbit anti-DOβ serum (39), and the Ii-specific polyclonal serum ICN2 (40) have previously been described. The Cy5 and horseradish peroxidase–conjugated secondary antibodies were from Sigma-Aldrich co. (Steinheim, Germany). Fluorescent secondary antibodies were from Molecular Probes (Leiden, The Netherlands).

DNA constructs and the generation of transfectants

A fusion construct between YFP and the C-terminus of DMα was generated by PCR. pcDNA3.1 Zeo vector (Invitrogen) was digested with *BamH*I and *Eco*RI and ligated to an IRES sequence, digested with *BamH*I and *Eco*RI, forming IRES pcDNA3.1 Zeo. IRES pcDNA3.1 Zeo was subsequently digested with *Eco*RI and *Xho*I. The digest was ligated with DMα-YFP, digested with *Eco*RI and *Xho*I, forming pcDNA3.1 Zeo IRES DMαYFP. pcDNA3.1 Zeo-IRES-DMα/YFP was subsequently digested with *Nhe*I and *Not*I and li-

gated with DMβ (41), digested with *Nhe*I and *Not*I in presence of 0.5% BSA, forming pcDNA3.1 Zeo-DMβ-IRES-DMαYFP.

Generation of a fusion construct between CFP and the C-terminus of DOβ (41) was achieved via PCR. pCEP4Δ vector (42) was digested with *Kpn*I and *Hind*III. The digest was ligated with DOα (43), digested with *Kpn*I and *Hind*III, forming pCEP4Δ DOα This construct was subsequently digested with *Eco*RV and *Nhe*I and ligated with IRES sequence, digested with *Eco*RV and *Nhe*I. Next, pCEP4Δ DOα-IRES was digested with *Nhe*I and *Xho*I and ligated with DOβCFP, digested with *Nhe*I and *Xho*I, forming pCEP4Δ DOα-IRES-DOβCFP. The same construct was generated without CFP attached to DOβ for use in HLA-DO overexpression experiments.

The fusion construct between CFP and the C-terminus of DR3β was generated via PCR. pcDNA3 DOβ/GFP vector (39) was digested with *Hind*III and *BamH*I and ligated with DR3β, digested with *Hind*III and *BamH*I, forming pcDNA3 DOα-GFP/DR3β. Subsequently, pcDNA3 DOα-GFP/DR3β was digested with *BamH*I and *Eco*RI and ligated with IRES, digested with *Eco*RV and *Nhe*I, forming pcDNA3 DRα-IRES. pcDNA3 DRα-IRES was subsequently digested with *Eco*RI and *Xho*I and ligated with DR3βCFP, digested with *Eco*RI and *Xho*I in Buffer H, forming pcDNA3 DRα-IRES-DR3β/CFP.

p30 invariant chain fragment was cut (*Eco*RI-*BamH*I) from Gem4sp6Ii vector and ligated blunt into the *Sma*I site of the pSV51L vector (gift from O.Bakke, Oslo). For selection, pSV51LIi was cotransfected with pcDNA3 ouabaine vector (44). GFP was swapped for CFP or YFP in H2B-GFP cloned in pcDNA3 (45) (by digestion with *Not*I and *BamH*I).

To generate the RNAi construct targeting the PIK3C3 gene (hVPS34), the RNAi vector pSUPER (46) was digested with *Bgl*II and *Hind*III and the annealed oligos containing the sequence AGTAGATTGGCTGGATAGA specific for hVPS34 were ligated into the vector.

Salmonella typhimurium strain SL1344 was transformed with a bacterial expression vector for mRFP (kind gift of R. Tsien). mRFP expressing bacteria were selected by fluorescence microscopy and further purified before use in tissue culture FRET experiments.

Human Embryo Kidney (HEK) 293 cells were stably transfected with DOα-IRES-DOβ/CFP, DRα-IRES-DR3β/CFP, DMβ-IRES-DMα/YFP, p30 invariant chain and/or pcDNA3 Ouabaine vector or left untransfected. These cells were grown on Dulbecco's modified Eagle's medium (DMEM) supplemented with 7.5% fetal calf serum (Gibco, Paisley, UK) in the presence or absence of 1000 µg/ml G418, 300µg/ml Hygromycin (Gibco, Paisley, UK), 500 µg/ml Zeocine (Invitrogen, Carlsbad, USA) and/or 2µM Ouabaine (Invitrogen, Carlsbad, USA), at 37°C in a humidified atmosphere containing 5% CO2. Stable expression of the CFP- and YFP-tagged proteins was ensured by regular selection of the CFP- and YFP-positive cells by FACS sorting. Stable transfectants of the melanoma cell line Mel JuSo (H2B-CFP, H2B-YFP) were grown in Iscove's medium with 7.5% FCS supplemented with 1000 µg/ml G418. For the HLA-DO competition experiments, 293 cells stably expressing HLA-DR3/CFP, HLA-DM/YFP and invariant chain were transiently transfected with DOαIRESDOβ and an empty vector mRFP vector (in 50:1 molar ratio) and analyzed 48 h after transfection.

Biochemical and Western Blot Analyses

Cell surface protein labeling was performed by lactoperoxidase-catalyzed iodination with 1mCi $Na^{125}I$ on cells grown to subconfluency in a 75-cm^2 tissue culture flask. Cells were washed four times with cold PBS, lysed in Tris-lysis buffer (pH 7.4) containing 0.5% NP-40 and 5mM $MgCl_2$, and used for immunoprecipitations with antibody recognizing MHC ClassII αβ complexes (Tü36). Samples were analyzed by 10% SDS-PAGE. Total protein expression levels were analyzed by growing HEK293 cells, stably transfected with HLA-DR3/CFP, HLA-DM/YFP,-DR/CFP, HLA-DM/YFP,-DR/CFP and Ii, HLA-DM/YFP,-DO/CFP or left untransfected, to subconfluency in Ø 10cm dishes. Cells were washed four times with cold PBS, lysed in Tris-lysis buffer (pH 7.4) containing 0.5% NP-40, 50mM Tris-HCl pH 7.4 and 5mM $MgCl_2$. Lysates were split into two halves. One was incubated in SDS-sample buffer at 95°C for 5 minutes, the other left at room temperature. Samples were separated by 10% SDS-PAGE, transferred to nitrocellulose and immuno-labeled with antibodies against GFP, HLA-DM, -DR, and -DO. To test for stability of the class II complex, boiled and unboiled samples were separated by 10% SDS-PAGE, transferred to nitrocellulose and incubated with antibody recognizing the DRα chain, both in the stable class II complex and as a free α chain (1B5). Equal amounts of protein were loaded.

CLSM and immuno-electronmicroscopy analysis

For CLSM analysis, coverslips were coated with 5µg/ml fibronectin (Sigma-Aldrich co., Steinheim, Germany) in PBS for 1h at 37°C. Subsequently, HEK293 transfectants were seeded on the coated coverslips. These were fixed with methanol and stained with anti-CD63 antibodies NKI-C3,

and secondary antibodies conjugated to Cy5. Images were taken with a Leica TCS SP2 System (Leica, Mannheim, Germany). HEK293 transfectants were fixed in a mixture of paraformaldehyde (4%) and glutaraldehyde (0.5%) prior to processing for immuno-electronmicroscopy. Cells were incubated with 200μM chloroquine for 3h or 6h before processing. For the *Salmonella* infection, *Salmonella* strain SL1344 was cultured o/n followed by renewed culture for 3h. For immuno-labeling, sections were incubated with purified mAb anti-human DMα (5C1), followed by incubations with rabbit anti-mouse IgG and 10nm protein A-conjugated colloidal gold. Subsequently, the sections were treated with 1% gluteraldehyde, followed by another incubation with rabbit anti-human class II serum and 15nm protein A-conjugated colloidal gold. After embedding in a mixture of methyl-cellulose and uranyl acetate, sections were analyzed with a Philips CM10 electron microscope (Eindhoven, the Netherlands).

Confocal FRET (CLSM-FRET) imaging by sensitized emission

The HEK293 transfectants were grown on the coated coverslips for 72h before imaging. 24h prior to imaging, Mel JuSo cells, stably transfected with H2B-CFP or H2B-YFP were added to the culture. Prior to CLSM, culture medium was changed for 2ml CBS medium (140mM NaCl, 5mM KCl_2, 2mM $MgCl_2$, 1mM $CaCl_2$, 23mM $NaHCO_3$, 10mM D-Glucose, 10mM Hepes pH 7.3) under 5% CO2, and the coverslips were analyzed in a heated tissue culture chamber at 37°C. Where indicated, chloroquine was added at a final concentration of 200μM for 2.5-3h or 6h prior to analysis. In the short-term pH neutralization experiments, the same cell was analysed prior to and directly after a 2' chloroquine treatment. For the RNAi experiments, cells were transfected with the pSUPER construct targeting hVPS34 and an empty mRFP vector as a transfection marker in a 10:1 ratio. 72h after transfection, mRFP positive cells were analyzed.

Fluorescence Resonance Energy Transfer between CFP and YFP molecules was studied by calculating the sensitized emission (the YFP emission upon CFP excitation) from separately acquired donor and acceptor images. Images were acquired on a DM-Ire2 inverted microscope fitted with TCS-SP2 scanhead (Leica, Mannheim, Germany). Three images were collected: CFP excited at 430nm and detected between 470 and 490nm; indirect YFP: excited at 430nm and detected between 528 and 603nm; and direct YFP excited at 514nm, and detected between 528 and 603nm. When simultaneously mRFP-*Salmonella* was monitored, CFP emission was detected between 455 and 510nm for noise reduction, and YFP emission was detected between 525 and 550nm to minimize leakage of mRFP signal into the YFP channel. mRFP was excited at 568nm, and detected between 582nm and 675nm. Remaining mRFP bleedthrough was eliminated by masking all pixels in the CFP, indirect YFP, and direct YFP images that corresponded to mRFP-positive pixels in the image taken of the mRFP-*Salmonellae*. Because of considerable overlap of CFP and YFP spectra, YFP emission was corrected for leak-through of CFP emission and for direct excitation of YFP during CFP excitation. FRET was calculated from these data as described in detail (47). In brief, the images were shade-corrected and optionally smoothed. Sensitized emission (F_{Sen}) was calculated using correction factors obtained from cells expressing either CFP or YFP alone, which were updated for every image. Then the apparent FRET efficiency was calculated by relating the F_{Sen} to the total donor level (E_D). See supplementary information for more details. Given the microscope used, the fluorescence intensities measured, and the number of pixels analyzed, FRET efficiencies as low as ~0.5% can be measured reliably (K.J. unpublished observations). Resulting FRET efficiency images were analyzed by plotting the CFP and YFP intensities for all pixels in a 2D plot, with the corresponding FRET efficiency in false colors. Using MatLab7 software (The Mathworks, Natick, USA) a mask was generated to select all pixels above the threshold set for both the CFP and YFP intensities (to exclude background fluorescence). For each pixel the CFP, YFP and FRET efficiency values were extracted and plotted using pro Fit 6 software (Quansoft, Uetikon am See, Switzerland). In case of the *Salmonella* experiments, pixels representing the SCV were extracted that 1) were contained within a region of interest drawn around the bacterium, 2) had intensities of both CFP and YFP that were above the set treshold to exclude background fluorescence, and 3) had a FRET efficiency of 0. Also for these pixels, the CFP and YFP values were extracted and plotted. For the E_D histograms shown in **Figure S8**, all pixels of an MIIC and SCV with a donor or acceptor fluorescent intensity between 10 and 250 were considered. Donor FRET efficiencies of these pixels were binned in 30 categories from -0.75 to +0.75 and plotted in a histogram.

Fluorescence Lifetime Imaging Microscopy

Fluorescence Lifetime Imaging (FLIM) experiments were performed on a Leica inverted DM-IRE2 microscope equiped with a Lambert Instruments frequency domain lifetime attachment (Leutingewolde, The Netherlands), controlled by the vendors EZflim software. CFP was excited at 430nm with ~4mW power using a LED modulated at 40MHz. Emission was collected at 450-490nm using an intensified CCD camera. Calculated CFP lifetimes were referenced to a 1μM solution of Rhodamine-G6 in medium that was set at 4.11ns lifetime, and calibrated using co-expressed H2B-CFP containing cells for which the lifetime was set to 2.7ns (48).

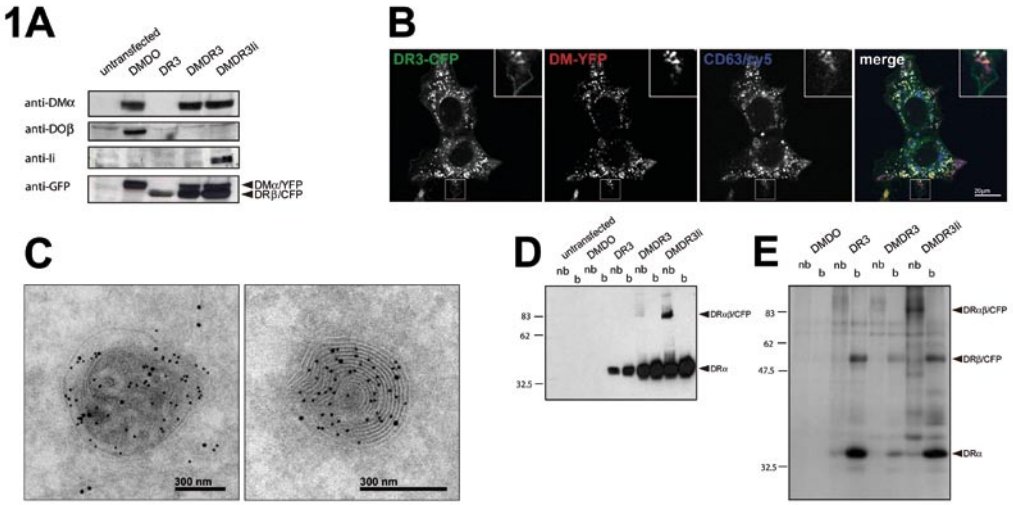

Figure 1. Characterization of the HEK293 Transfectants Expressing HLA-DR3/CFP and HLA-DM/YFP

(**A**) HEK293 cells expressing DM/YFP, DO/CFP, DR3/CFP, and the invariant chain (Ii) were analyzed by SDS-PAGE and Western blotting with the antibodies indicated.

(**B**) Intracellular distribution of DR3/CFP and DM/YFP in Ii-expressing HEK293 cells. Cells were fixed and stained with anti-CD63 antibody, and the various fluorophores were analyzed as indicated. A strong colocalization between DR3, DM, and CD63 is observed. Inset shows the selective surface expression of DR3/CFP.

(**C**) DR3/CFP and DM/YFP localize to multivesicular and multilamellar structures. HEK293 cells expressing DR3/CFP, DM/YFP, and Ii were fixed and prepared for cryo-immuno-EM. DM (10 nm gold) and DR3 (15 nm gold) localize to both the internal structures and the limiting membrane of MIIC.

(**D**) Analysis of DR3/CFP peptide loading. Lysates of the different transfectants were incubated in SDS-loading buffer and split in two. One half was boiled at 100°C for 5 min (lanes "b" for boiled) and the other left at room temperature (lane "nb" for nonboiled) before separation by SDS-PAGE. Proteins were transferred to nitrocellulose and stained with antibody against DRα chain. Free DRα (35 kDa) and DRαβ/CFP complexes (83 kDa) are indicated. Compact, DR3/CFP-peptide complexes are only detected when cells coexpress DM/YFP and Ii.

(**E**) Analysis of cell surface-expressed MHC class II complexes. The various transfectants were cell surface iodinated and MHC class II complexes were immune precipitated. The immune isolates were either boiled in SDS loading buffer (lanes "b") or left at room temperature (lanes "nb") before separation by SDS-PAGE. The position of DRα, DR3β-CFP and the DR3αβ/CFP-peptide complex is indicated. Compact, DR3/CFP-peptide complexes are only detected at the plasma membrane when cells coexpress DM/YFP and Ii.

Subcellular fractionation

HEK293 transfectants were infected with *Salmonella* for 4h. Cells were washed with PBS and scraped from the plate prior to dounching by an EMBL Cell Cracker. Debris was removed by a low spin centrifugation step and the post-nuclear supernatant was loaded on a 0.4-2.4M step-wise sucrose gradient (steps of 0.4M) in 10µM Tris-HCl pH8.0. This was centrifuged for 3h in a swing-out rotor (Beckman 40.1Ti) at 28.000 rpm. 0.5ml samples from the gradient were diluted 1:1 with PBS and 200µl was used in a standard β-hexosaminidase assay. The rest of the vesicles was pelleted by centrifugation (15 min, 12.000g), and incubated in SDS-loading buffer for 5 min at room temperature prior to separation by 10% SDS-PAGE and Western blotting.

Results

A System to Monitor HLA-DR3 Interaction with DM

To study the interaction between DR and DM, the molecules were tagged with two variants of the Green Fluorescent Protein (GFP): Cyan Fluorescent Protein (CFP) attached to the cytoplasmic tail of DR3β and Yellow Fluorescent Protein (YFP) linked to the cytoplasmic tail of DMα. GFP tagging of the DR3β chain has been successfully used before but without measurable effects on MHC class II behavior (49, 50). The DMβ chain contains the lysosomal-targeting information (51), therefore the DMα chain was used for YFP tagging. To investigate whether the various

modifications still allowed a productive interaction between DR3/CFP and DM/YFP, the DRα and DR3β/CFP chains were stably expressed into Human Embryonic Kidney (HEK) 293 cells along with the DMα/YFP and DMβ chains. We generated three cell lines: HEK293 cells expressing only DR3/CFP, HEK293 cells expressing DR3/CFP and DM/YFP, and HEK293 cells expressing DR3/CFP, DM/YFP, and the p30 form of the invariant chain (Ii). By introducing these chains in a nonimmune cell line, DR3/CFP peptide loading could only be supported by YFP-tagged DM because no endogenous DM was present. First, expression of the various subunits was confirmed by Western blotting (**Figure 1A**). Subsequent analysis of the stable cell lines by Confocal Laser Scanning Microscopy (CLSM) revealed that DM/YFP was efficiently targeted to endosomal structures, whereas DR3/CFP was mainly retained in the ER unless the invariant chain was coexpressed (**Figure S1** in the Supplemental Data). In the presence of the invariant chain, DM/YFP and DR3/CFP were both efficiently transported to endosomal structures containing CD63 as a marker, and DR3/CFP arrived at the plasma membrane with similar efficiency as observed in cells endogenously expressing DR3 (**Figures 1B** and **S2**). These endosomal compartments had the characteristic morphology of MIIC and were a mixture of multilamellar and multivesicular bodies, as shown by immuno-electron microscopy (EM) (**Figure 1C**). Note that DM/YFP and DR3/CFP were both distributed over the limiting membrane and the internal vesicles of the MIIC.

Peptide loading was assayed biochemically. DR3 with high affinity peptides will not dissociate in SDS-loading buffer when incubated at room temperature, resulting in slower migration of the so-called compact form by SDS-PAGE analysis (52, 53). A substantial amount of compact DR3/CFP molecules was detected only when DM/YFP and the invariant chain were coexpressed (**Figure 1D**). This was confirmed by surface iodination and analysis of DR3/CFP for temperature stability (**Figure 1E**). DM/YFP supported peptide loading of DR3/CFP, implying that the CFP/YFP modifications did not prevent a successful interaction between the two partners. Since the expression, distribution, MHC class II loading with peptides, and transport to the plasma membrane mimicked the situation in antigen presenting cells, we continued our studies with the HEK293 cells stably transfected with DR3/CFP, DM/YFP, and the invariant chain.

FRET Analyses and the Interaction of HLA-DM with HLA-DR3 or HLA-DO

FRET is the radiationless transfer of energy from an excited donor fluorophore to a suitable acceptor fluorophore, a physical process that depends on spectral overlap and proper dipole alignment of the two fluorophores. The occurrence of FRET between CFP and YFP is characterized by a decrease in CFP emission, and simultaneously sensitized (increased) YFP emission. Importantly, FRET is extremely sensitive to the distance between the fluorophores (its efficiency decays with the distance to the sixth power) (54). For CFP and YFP, the characteristic half-maximum distance is 49–52 Å (Förster radius) with an upper limit of 80 Å (55). Given the dimensions of GFP and its color variants (56), DM (57), and DR3 (58), FRET between DR3/CFP and DM/YFP will only occur when both proteins are no more than one molecule in distance apart (**Figure 2**). Thus, if FRET is observed, DM almost certainly interacts with DR3.

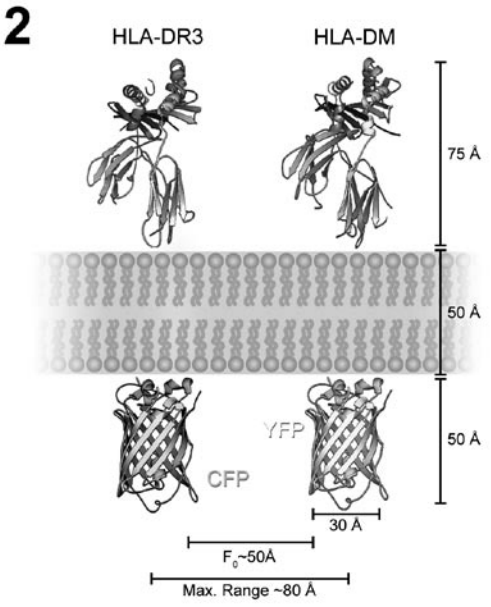

Figure 2. Dimensions of HLA-DR3/CFP, HLA-DM/YFP, and FRET. The structures of DR and DM are projected above a membrane of about 50 Å thick. The transmembrane regions of both molecules are undefined and not shown. CFP and YFP have a barrel shape of 30 × 50 Å with a fluorescent moiety inside. Shown are both the maximal distance (80 Å) that can be detected by fluorescence resonance energy transfer (FRET), and the Förster radius (F_0), the distance at which FRET between CFP and YFP is half maximal (50 Å).

FRET was studied by calculating the sensitized emission from confocal CFP and YFP images, as described in depth (59). Leakthrough factors (due to spectral overlap of the fluorophores) were calculated from cells expressing histon 2B (H2B) coupled to CFP or YFP that were cocultured with the cells under study (see Supplemental Data). No FRET signal of H2B-CFP and H2B-YFP should be observed in the final (fully corrected) sensitized emission pictures. **Figure 3A** shows a representative example of our experimental procedure using CLSM-FRET. The H2B-C/YFP expressing control cells could be easily recognized by their nuclear fluorescence. Sensitized emission (further referred to as 'FRET') between DM and DR3 was only detected in vesicles, as the algorithm used to correct for leakthrough terms effectively removed both the DR3 signal at the plasma membrane and the nuclear H2B-C/YFP fluorescence (**Figure 3A**, panel FRET).

The efficiency of DR3 interactions with DM was deduced from the donor FRET efficiency (E_D), the FRET signal relative to the amount of donor fluorescence, which is DR3/CFP. A donor FRET efficiency of 5.3% was detected, far above the minimal efficiency detectable by this technique (see **Supplemental Data**). Little variation was observed between the various MIIC structures within one cell (**Figure 3A**, panel E_D) and in cells with different ratios of DR3/CFP versus DM/YFP, suggesting saturating amounts of DM/YFP for the catalysis of peptide loading of DR3/CFP in these vesicles (**Figure S3** in the Suppl. Data). This was further visualized by plotting for each pixel the FRET efficiency versus the DR3/CFP and DM/YFP intensities (**Figure 3E**). No correlation was observed between FRET efficiency and the intensity of CFP and YFP, showing that this represented true interactions rather than accidental collision of both proteins.

GFP and its color variants can be sensitive to the environment, for example to hydrophobicity and pH (55). Because they are situated in acidic vesicles with many membranes, alterations in FRET could be the result of an altered environment in which the CFP/YFP molecules reside. As a control, we generated a stable HEK293 cell line expressing DM/YFP and DO/CFP. DO is homologous to DR (DOβ shares 75% amino acid sequence identity with DR3β), but unlike DR, interacts stably with DM. Consequently, if a change in FRET efficiency between DO and DM is observed, this could be the result of an altered environment of the fluorophores. DO is targeted mainly by DM to MIIC and is virtually absent from the plasma membrane. DO/CFP and DM/YFP localized to the same late endocytic, CD63-containing structures as DM/YFP and DR3/CFP, as shown by CLSM (**Figure 3B**) and immuno-EM with anti-GFP antibodies (**Figure 3C**). As observed before (60), DM/YFP, DO/CFP was mainly located on the limiting membrane but also on internal structures of characteristic multivesicular/multilamellar MIIC. These DM/YFP, DO/CFP cells were used as controls in further experiments.

FRET was measured between DO and DM under conditions identical to those described for Figure 3A. Efficient FRET was detected between these molecules (**Figure 3D**). The FRET efficiency for the interaction between DO and DM was 23.2% (SD = 3.5%) compared to 5.3% (SD = 1.5%) observed for DR3 and DM (**Figure 3F**), and is obviously not affected by acceptor (YFP) concentrations (**Figure 3E**). This ratio in FRET efficiency was determined by both wide field (data not shown) and CLSM-FRET and confirmed by FLIM (Fluorescence Lifetime Imaging Microscopy) analysis, an alternative technique to monitor FRET (61). The lifetime (the average duration of the excited state) for the donor CFP is typically 2.7 ns (62) but is reduced when energy is transfered to YFP following the same rules for FRET as described earlier. FLIM offers the advantage that it reports FRET in a highly quantitative manner, but as implemented here, lacks confocal sectioning capacity. Also, it requires relatively long sampling times (12s) to accurately determine the lifetime of the fluorophore (a problem for moving vesicles). **Figure 3G** shows wide-field FLIM measurements of the DM/YFP and DR3/CFP or DO/CFP cells, cocultured with the H2B-CFP-containing Mel JuSo cells in the presence of nocodazole to block vesicle transport. Arrows indicate examples of vesicles that were immobile during the measurement. The DR3/CFP lifetime was on average 2.49 ns in the presence of DM/YFP, and 1.52 ns in that of DO/CFP. These values correspond to a FRET efficiency ratio of 1:5.6 ([2.7 − 2.49]/[2.7 − 1.52]), similar as detected with CLSM-FRET.

The higher FRET efficiency between DM and DO is not surprising because these molecules continuously interact, whereas DM will interact transiently with DR3 as long as the class II molecule contains CLIP or another nonstably binding peptide. Together, these data show that we have established a cell system to follow interactions between DR3 and its dedicated chaperone DM in MIIC of living cells by FRET.

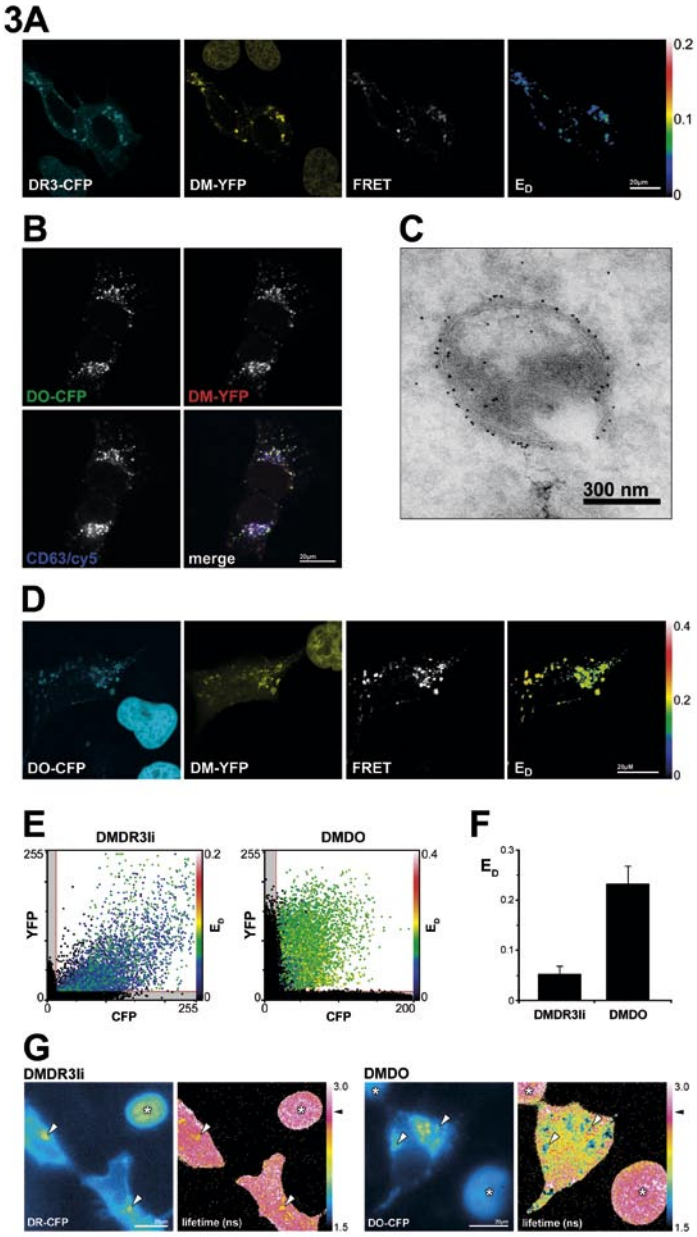

Figure 3. FRET Measurements

(**A**) FRET between DR3/CFP and DM/YFP with internal controls by CLSM. HEK293 cells with DR3/CFP, DM/YFP, and Ii were cocultured with Mel JuSo cells expressing H2B-CFP or H2B-YFP, and FRET was measured in living cells at 37°C. Nuclear fluorescence identifies control cells. After correction for fluorescent leakthrough (see Experimental Procedures), FRET between DR3 and DM is observed as sensitized emission (panel "FRET"). The efficiency of interaction is shown in false colors by the donor FRET efficiency, the FRET signal related to the amount of donor fluorescence (panel "E_D"). DR3/CFP is located in MIIC and at the plasma membrane, and DM/YFP only in MIIC. FRET between these complexes is solely observed in the endosomal structures. The relative FRET efficiency values corresponding to the respective colors are indicated.

(**B**) Intracellular distribution of DO/CFP and DM/YFP in HEK293 cells. The stable transfectants were methanol fixed, incubated with anti-CD63 antibodies labeled with Cy5, and analyzed by CLSM. DM/DO colocalizes with CD63 in endosomal structures.

(**C**) Distribution of DO/CFP and DM/YFP in MIIC. HEK293 cells transfected with the DO/CFP and DM/YFP were fixed, and sections were labeled with anti-GFP antibodies before analysis by immuno-EM. GFP labeling is observed at the limiting membrane and in internal structures.

(**D**) CLSM-FRET with internal controls of living HEK293 cells expressing DO/CFP and DM/YFP. The protocol is described under (A). High donor FRET efficiency (E_D) is observed between DO and DM in endosomal structures. (**E**) Analysis of FRET efficiency images. From the images in (A) and (D), CFP, YFP, and FRET efficiency values were extracted for all pixels and plotted on the x and y axis, respectively, with corresponding FRET efficiencies (E_D) depicted in the false colors. The threshold set to exclude background fluorescence is indicated with a red line. (**F**) Quantification of the donor FRET efficiency (E_D). E_D observed in endosomal structures between DR3/CFP and DM/YFP, and between DO/CFP and DM/YFP was determined in, respectively, 16 and 11 individual experiments made on various days. (**G**) FLIM measurements of the interactions between CFP/YFP-labeled DR3 and DM, or DO and DM in HEK293 cells, cocultured with H2B-CFP internal controls and treated with nocodazole to disrupt vesicle transport. Fluorophore excited state lifetime decreases upon FRET. Left panel shows wide field CFP fluorescence, right panel shows calculated lifetime (in ns) in false colors. The average lifetime of CFP in the absence of FRET (2.7 ns) is indicated with a black arrowhead. Only vesicles immobile during data sampling (12 s) were considered, of which two examples are indicated in both images by white arrowheads. These vesicles had a shorter CFP lifetime than the H2B-CFP controls (indicated by asterisk).

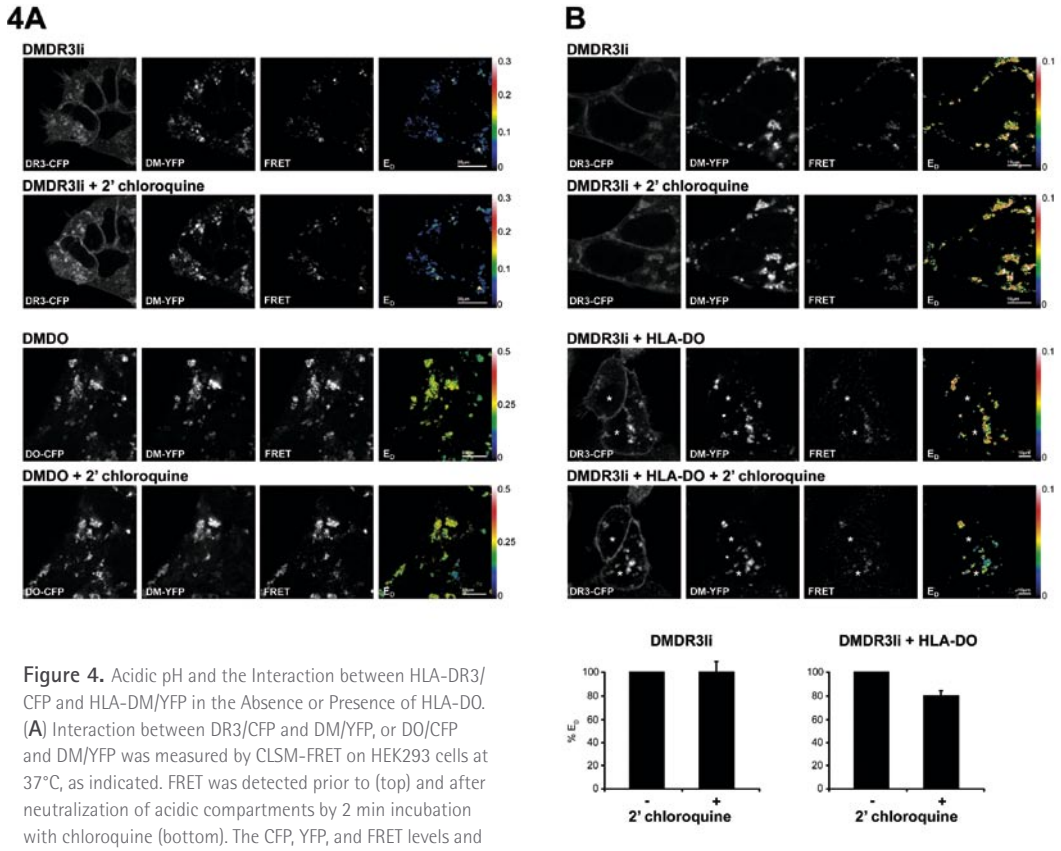

Figure 4. Acidic pH and the Interaction between HLA-DR3/CFP and HLA-DM/YFP in the Absence or Presence of HLA-DO. (**A**) Interaction between DR3/CFP and DM/YFP, or DO/CFP and DM/YFP was measured by CLSM-FRET on HEK293 cells at 37°C, as indicated. FRET was detected prior to (top) and after neutralization of acidic compartments by 2 min incubation with chloroquine (bottom). The CFP, YFP, and FRET levels and donor FRET efficiency (ED) were determined (details in Figure 3A). FRET between DR3/CFP and DM/YFP is not affected by chloroquine treatment, and neither did neutralization affect DO and DM (n > 50 independent measurements). (**B**) The interaction between DR3/CFP and DM/YFP becomes pH dependent upon DO expression. The same analysis as in (A) was performed on the DR3/CFP, DM/YFP and invariant chain-expressing HEK293 transfectants (upper panel), and the same cells overexpressing unlabeled DO with H2B-mRFP as a transfection marker (lower panel). The H2B-mRFP signal is not shown (see Figure S5). Interaction between DR3/CFP and DM/YFP is not affected by DO expression at normal acidic pH but is reduced upon neutralization with chloroquine. FRET efficiencies measured on the identical vesicles prior to and after neutralization are depicted in the bar diagrams with the SD indicated (n > 50 pairwise measurements).

HLA-DR3 Interactions with HLA-DM Are Not pH Dependent *In Vivo* Unless HLA-DO Is Present

The interaction between DM and DR3 is sensitive to pH, at least *in vitro*. DM-mediated peptide exchange on DR is optimal at pH 4.5 and about 4 times less efficient at pH 7 (63). Also, DM can only be coisolated with DR at acidic pH (8). Furthermore, prolonged incubation with lysosomotropic agents like NH_4Cl and chloroquine inhibits MHC class II antigen presentation (25). We tested whether neutralization of MIIC by two minutes of chloroquine treatment (**Figure S4** in the Supplemental Data) affected the interaction between DM and DR3 *in vivo* in intact MIIC, as could now be visualized by FRET. The DM/YFP, DO/CFP cells were taken to control for potential influences of pH changes on the fluorophores. Neutralization of acidic structures did not affect FRET efficiency between DM and DO but, surprisingly, neither between DR3 and DM (**Figure 4A**). Only when the pH sensor DO (63) was overexpressed in the DR3/CFP, DM/YFP cells (**Figure S5** in the Supplemental Data), a reduction in FRET efficiency between DR3 and DM was observed upon chloroquine treatment (**Figure 4B**). Overexpression of DO apparently does not change the relative orientation of DM to DR3, at least not at acidic pH, suggesting that DO does not act as a DR mimmick, but merely as a pH sensor for DM-

mediated peptide loading of DR (63). Still, there is an apparent discrepancy between the *in vitro* experiments where DR and DM require acidic pH for activity and the *in vivo* FRET data. Possibly, DR3 and DM localize in microdomains within the MIIC that stabilize their interaction, even under conditions of neutral pH.

Spatial Differences within MIIC Affect HLA-DR3 Interactions with HLA-DM

It has been known for over 20 years that long-term treatment with chloroquine or NH_4Cl induces swelling of lysosomes (64). We demonstrate that the membranes needed for swelling are provided by internal vesicles that fuse back to the limiting membrane. This is concluded because 1. MIIC swelled after chloroquine treatment in our transfectants under conditions that vesicle transport was blocked (by destroying the microtubular network with nocodazole), and consequently, input of new membrane material was prevented (**Figure S6** in the Supplemental Data, inset). Membranes for the expanding limiting membrane can only be supplied by the internal structures under this condition. 2. Markers for internal vesicles like CD63 were found at the limiting membrane after long-term chloroquine treatment (data not shown). 3. Electron Microscopy (EM) showed that the swollen MIIC did not contain internal vesicles after 4–6 hr chloroquine treatment because these had supplied the material for the expanding limiting membrane. Indeed, also DR3/CFP and DM/YFP were located at the limiting membrane by immuno-EM (**Figure 5A**) and CLSM (**Figure 5B**) in structures without internal vesicles. Thus, long-term chloroquine treatment, which is known to prevent MHC class II antigen presentation, appears to alter the architecture of an MIIC structure by backfusion of the internal vesicles with the limiting membrane.

We made use of this MIIC remodeling in subsequent experiments in which the interaction between DM and DR3 (and between DM and DO as a control) was measured in cells treated for 6 hr with 200 μM chloroquine (**Figure 5B**). The interaction (as visualized by CLSM-FRET) between DM and DO was not affected on swollen late-endosomal structures (middle panel), whereas DM and DR3 did not interact on the limiting membrane (the only membrane) of these structures (upper panel). The concentration of DR3/CFP and DM/YFP does not decrease when the expansion of MIIC is the result of backfusion of internal structures. This implies that the FRET observed in Figure 3A and Figure 4A was not caused by coincidental collisions but resulted from more stable interactions. This suggested that interactions between DR3 and DM in MIIC occur exclusively at the internal structures.

The size of MIIC (~500 nm) is too small to distinguish between limiting and internal membranes by light microscopy. The swelling of MIIC by chloroquine occurs gradually. Therefore, we expected to obtain partially swollen structures with internal vesicles 2–3 hr after chloroquine addition, providing sufficient spatial resolution to distinguish internal and limiting membranes by CLSM-FRET. Immuno-EM 3 hr after chloroquine treatment showed swollen structures of around 1–2 μm with internal vesicles still containing DR3 and DM molecules (**Figure 5C**). These MIIC were sufficiently large to resolve internal and limiting membranes by CLSM, and FRET between DR3/CFP and DM/YFP in the partially swollen MIIC was measured (**Figure 5D**, upper panel). Although DM and DR3 are both present on the limiting and internal membranes, a substantial interaction was only observed in the internal structures and not at the limiting membrane. To exclude a decrease in DM and/or DR3 concentration due to the addition of membranes derived from fused vesicles, we repeated the experiment on nocodazole treated cells. This gave identical results (**Figure S6** in the Supplemental Data). As a control, DM and DO showed FRET at both the limiting and internal membranes under identical conditions (**Figure 5D**, middle panel). These data indicate that MIIC are not homogeneous structures but that they contain various subdomains that allow a productive interaction between DM and DR3 only on the internal structures but not the limiting membrane.

Inhibition of Formation of Internal Structures Prevents the Interaction between HLA-DR3 and HLA-DM

The PI3-kinase VPS34 is required to initiate a cascade of events resulting in recruitment of ESCRT complexes and ultimately formation of internal structures within multivesicular bodies (23). Inhibition of hVPS34, either genetically or with chemical inhibitors (24), results in swollen structures only containing a limiting membrane. Inhibition of hVPS34 would thus be an alternative to recruit DR3/CFP and DM/YFP to the limiting membrane. However, unlike the situation for chloroquine, the structures remain acidic (**Figure S7** in the Supplemental Data). An RNAi construct targeting hVPS34 was cotransfected with mRFP in HEK293 cells expressing DR3/

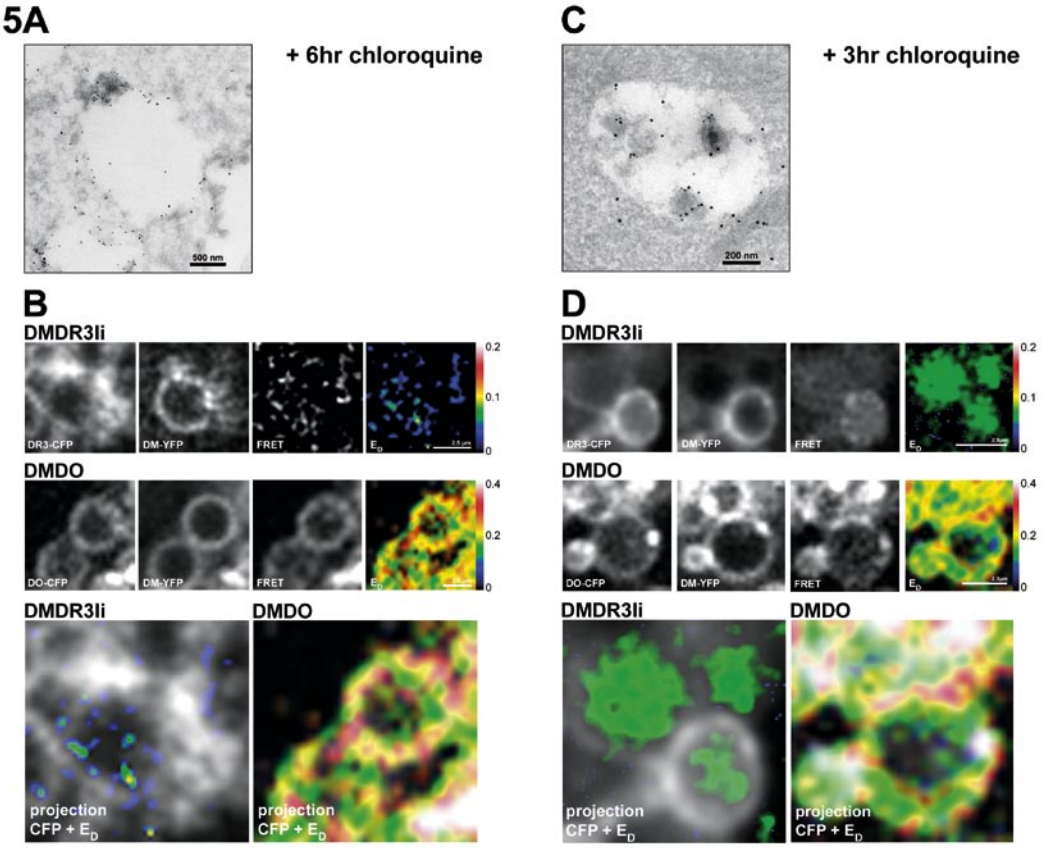

Figure 5. HLA-DR Interactions with HLA-DM on the Internal Structures of MIIC.
(**A**) Six-hour chloroquine treatment relocalizes DR3/CFP and DM/YFP to the limiting membrane of empty expanded MIIC. HEK293 cells expressing DR3/CFP, DM/YFP, and Ii were processed for cryo immuno-EM after 6 hr incubation with chloroquine. DR3, 15 nm gold; DM, 10 nm gold. Both proteins localize to the limiting membrane in structures lacking internal vesicles.
(**B**) DR3/CFP does not interact with DM/YFP at the limiting membrane. HEK293 cells expressing DR3/CFP, DM/YFP, and Ii (upper panel) or DO/CFP and DM/YFP (middle panel) were analyzed by CLSM-FRET at 37°C after 6 hr of chloroquine treatment. The CFP, YFP, FRET levels, and donor FRET efficiency (E_D) were determined (details in Figure 3A). The lower panel shows the E_D in false colors projected on the CFP signal in white. Whereas DM and DO interact on the limiting membrane, no interaction is observed for DR3 and DM (n > 50 observations).
(**C**) The structure of partially swollen MIIC after 3 hr chloroquine treatment. HEK293 cells expressing DR3/CFP, DM/YFP and Ii were cultured for 3 hr in the presence of chloroquine before analysis by cryo immuno-EM. Swollen MIIC are observed still containing internal structures. DR (15 nm gold) and DM (10 nm gold) are located on both the internal vesicles and limiting membrane.
(**D**) DR3/CFP interacts with DM/YFP on the internal structures of MIIC. Living HEK293 cells transfected with DR3/CFP, DM/YFP, and Ii (upper panel) or DO/CFP, DM/YFP (middle panel) were analyzed by CLSM-FRET at 37°C after 3 hr of chloroquine treatment. Panels are organized identical as in (B). Whereas DM and DO interact on both the internal structures and the limiting membrane, DR3 and DM only interact on the internal structures (n > 100 observations).

CFP, DM/YFP, and the invariant chain, as well as in cells expressing DO/CFP and DM/YFP as a control. Only mRFP-positive cells were analyzed for swollen structures, and FRET and donor FRET efficiency was determined (**Figure 6**). Whereas DM/YFP and DO/CFP showed FRET with normal efficiency, no FRET was detected between DR/CFP and DM/YFP at the limiting membrane of these swollen structures, analogous to the situation where MIIC was expanded by chloroquine (**Figure 5**). In conclusion, two treat-

ments known to inhibit antigen presentation by MHC class II molecules (26, 65) also induce localization of DR3 and DM to the limiting membrane of MIIC, where the interaction between these two proteins is prevented (**Figure 6**).

HLA-DR3 Interactions with HLA-DM and Peptide Loading on Phagosomal Membranes

If DR3 and DM fail to interact efficiently on limiting membranes, this may explain examples of immune escape observed under physiological conditions. In particular, bacterial pathogens like *Mycobacterium tuberculosis* and *Salmonella typhimurium* survive and propagate in acidified, self-induced phagosomes often unnoticed by the immune system (30). Phagosomes contain a limiting membrane only, unless the pathogen is killed. Recently, it has been shown that *Salmonella* secretes the PIP_2-phosphatase SopB into the cytoplasm of infected cells that hydrolyzes a downstream product of hVPS34 ($PI(3,5)P_2$), thus inducing phagosome formation (33). Hence, is the interaction between DR3 and DM inhibited at the phagosomal membrane? We infected HEK293 cells expressing DR3/CFP, DM/YFP and invariant chain with *Salmonella* for 4 hr and processed the cells for immuno-EM (**Figure 7A**, left panel). Intracellular *Salmonella* was found in a typical phagosome (termed the *Salmonella*-containing vacuole or SCV), containing DR3 and DM at the limiting membrane. No internal vesicles were found unless the bacterium was degraded (**Figure 7A**, right panel). Conventional, unaffected MIIC were also found in the same cell (**Figure 7A**, left panel insert). Next, we determined whether FRET between DR3/CFP and DM/YFP could be detected in SCV. As a control, we measured FRET between DM/YFP and DO/CFP on the same compartment. To allow simultaneous visualization of the intracellular bacteria, we generated mRFP-expressing *Salmonellae*. **Figure 7B** shows CLSM-FRET images of SCV and MIIC after 4 hr *Salmonella* infection in cells expressing DM and DO. The interaction between DO/CFP and DM/YFP was not affected on the phagosomal membrane. The interaction of DM and DR3 on SCV is shown in **Figure 7C**. To exclude the possibility that FRET between DR3/CFP and DM/YFP was not observed because their fluorescent intensities fell below the treshold set for background fluorescence, we analyzed the data in **Figures 7B** and **7C** by the same 2D-intensity plot approach used in Figure 3E. In addition, the CFP and YFP intensities of the pixels corresponding to the limiting membrane of the SCV where FRET was not detected are indicated in purple (**Figure 7D**). The limiting membrane of SCV contained hardly any pixels without FRET between DO/CFP and DM/YFP (resulting in only few purple dots in the middle panel). In contrast, pixels lacking FRET efficiency at the SCV membrane were abundantly found in the DR3/CFP, DM/YFP cells. The intensities of CFP and YFP in the majority of these SCV pixels corresponded to those found for MIIC in the same cell with positive FRET efficiencies. This analysis was repeated by considering the poisson-distributed noise for the calculated E_D per pixel (**Figure S8** in the Supplemental Data). Collectively, these data show an equally efficient interaction between DO and DM in MIIC and SCV, whereas the interaction between DR3 and DM was only observed in the MIIC and not the SCV membrane. Thus, within the same cell, two types of MHC class II-containing compartments were found: MIIC, where DM and DR3 could engage in antigen loading, and SCV, where DM and DR3 were prevented from interacting. MIIC vesicles showed continuous kiss-and-run type of contacts with the SCV (data not shown) but no DM/DR3 interaction was observed on the limiting membrane in more than 60% of the SCV (41 negative, 25 positive SCVs, n = 66). When *Salmonella* was intracellularly degraded, internal structures reappeared (**Figure 7A**, right panel), probably leading to some SCVs with detectable FRET between DM and DR3. Thus, the interaction between DR3 and DM was obstructed in intact phagosomal structures, similar to the situation in swollen MIIC, apparently because the microenvironment of internal endosomal membranes is a prerequisite for this interaction.

Is the loading of MHC class II molecules in SCV affected, as would be predicted from the FRET data? HEK293 cells expressing DR3/CFP, DM/YFP, and the invariant chain were infected with *Salmonella* for 4 hr before subcellular fractionation. Twenty percent of each fraction was used to measure β-hexosaminidase activity to position the late endosomes and lysosomes (**Figure 7E**, upper panel). The rest was incubated in SDS sample buffer at room temperature before separation by SDS-PAGE and Western blotting. This procedure should allow detection of compact type, SDS-stable, peptide-loaded DR3/CFP molecules (52). The nitrocellulose filter was probed sequentially with antibodies directed against the DRα chain and DR3αβ-peptide complex, against GFP, MHC class I molecules, and against a 30 kDa *Salmonella* protein. The position of the various proteins is given in the

compilation (**Figure 7E**, lower panel). MHC class I marks the plasma membrane and ER (fraction 6,7), β-hexosaminidase and DMα-YFP the MIIC (fractions 5,6), and the *Salmonella* protein the SCV (fractions 9,10). SCV contained both DM/YFP and DR3/CFP, as was also shown by CLSM and EM (**Figures 7A–7C**). Still, whereas a large portion of DR3/CFP was in a compact state in the plasma membrane and MIIC-containing fractions, hardly any peptide-loaded DR3 molecules were observed in SCV (compare lanes 5 and 9 in **Figure 7E**). Peptide loading of DR3 in SCV was apparently very inefficient, corresponding with the poor interaction observed between DM and DR3 on the limiting membranes of SCV and MIIC.

Discussion

The MIIC was defined in 1991 as a late endosomal compartment with a multilamellar morphology containing MHC class II molecules (2). Since then, a number of factors have been defined, notably cathepsins (66) and DM (4, 6), required for successful antigen loading of MHC class II molecules. The localization of DM to MIIC defined it as the major site for antigen loading of MHC class II molecules (67). The interaction between DM and MHC class II molecules has been shown *in vitro* and by coisolation (8, 10, 12). Critical for this interaction is acidic pH, as expected for a late-endosomal chaperone. How DM and DR interact in living cells has been unclear. For this reason, we generated cells expressing DR3 conjugated to CFP and YFP-labeled DM. DR3/CFP required the invariant chain for efficient release from the ER and transport to MIIC. The CFP/YFP modifications did not block peptide loading of DR3 because compact, SDS-stable, DR3/CFP molecules were formed with the support of DM/YFP. Next, we studied the interaction between DR3 and DM in living cells by FRET analysis. As a control, we used a cell line expressing DM/YFP and DO/CFP. DO is very similar to DR3 but stably interacts with DM. Because of their high similarity, DO may mimic DR for DM molecules. However, since overexpressed DO does not affect the FRET efficiency between DR3 and DM, this is unlikely. DO is apparently not a competitor for DR3 binding to DM but probably binds at another site thus affecting the (pH-dependent) chaperoning activity of DM.

The internal membranes of the MIIC have a different protein and lipid composition than the limiting membrane. DM and DR can be found in both endosomal subcompartments, albeit in variable amounts (17). We have investigated DR/DM interactions in the MIIC by FRET. Like their untagged counterparts, the DR3/CFP and DM/YFP molecules localized to both the internal structures and the limiting membrane, but FRET between these molecules was only seen on the internal structures. In order to optically separate internal and limiting membranes, the MIIC was swollen by chloroquine treatment. Chloroquine induces the fusion of internal structures with the limiting membrane, which subsequently expands at the cost of the internal structures. Long-term treatment with chloroquine completely depleted the internal structures and DR3 and DM resided at the limiting membrane where they failed to interact. Chloroquine treatment is a common way to inhibit (most) MHC class II responses. This could be the result of decreased antigen degradation by lysosomal proteases due to neutralization (although most cathepsins are active at neutral pH), less efficient support by DM (yet we show that the interaction with DR3 is not disturbed by neutralization), but may also be the result of repositioning DM and DR3 to the limiting membrane where they do not interact.

How is the interaction between DM and DR3 supported at the internal structures? Obvious candidates are the tetraspans CD63 and CD82, given their almost exclusive location in the internal structures and their interaction with MHC class II and DM (20, 21). It has been suggested that microdomain clusters of DR/DM and the tetraspans could have different peptide loading properties (22). However, the tetraspans CD63 and CD82 are also relocated to the limiting membrane following chloroquine treatment (not shown) where DR3 and DM do not interact. Thus, the tetraspans CD63 and CD82 are not sufficient, if at all required, for stable DR3/DM interactions. Whether other proteins or lipids are involved in the formation of a putative "MHC class II loading microdomain" inside the MIIC, is as yet unclear.

Phagosomes are endosomal structures where intracellular bacteria survive and even propagate. Morphologically, these structures resemble a swollen MIIC, and can be considered a limiting membrane around the bacterium. Various studies describe the effect of intracellular bacteria on antigen presentation. $CD4^+$ T cells can be easily isolated after most bacterial infections, but it is unclear whether this is a response to a killed bacterium or a viable one. *In vitro* T cell assays yield mixed conclusions (68). T cell responses against

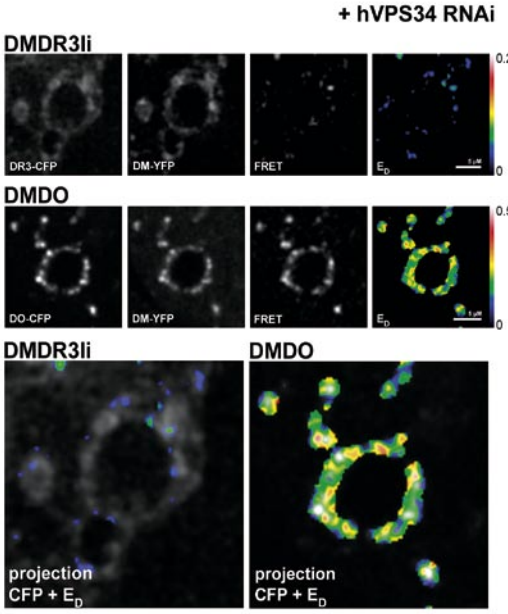

Figure 6. Inhibition of MVB Formation and the Interaction of HLA-DR3 with HLA-DM. HEK293 cells expressing DR3/CFP, DM/YFP and Ii, or DO/CFP and DM/YFP were transfected with two constructs encoding the RNAi for hVPS34 and soluble mRFP, respectively. After 72 hr, living cells expressing mRFP (not shown) with swollen MIIC were analyzed. A zoom-in of an expanded structure is shown. The CFP signal, YFP signal, FRET, and donorFRET efficiency (E_D) measurements are indicated (details in Figure 3A). The lower panel shows the E_D projected in false colors on the CFP signal in white. Whereas both DR3/CFP and DM/YFP are present at the limiting membrane of the expanded MIIC, they do not interact (n > 50 independent measurements).

other antigens coincubated with the bacterium are usually not affected, although some infections can reduce or inhibit antigen presentation by MHC class II (69). Whereas various bacteria neutralize phagosomes, *Salmonella* allows acidification, which is even required for the secretion of effector proteins (70).

Salmonella apparently forms phagosomes by secreting a PIP_2-phosphatase, SopB, thus inactivating the hVPS34-ESCRT system of internal vesicle formation (33). Likewise, *M. tuberculosis* toxin directly inactivates hVPS34 (32). Downregulation of hVPS34 by RNAi induced expanded MIIC and prevented the interaction between DR3/CFP and DM/YFP on the limiting membrane. This also inhibits antigen presentation by MHC Class II (26). In addition, the expression of DM/YFP and DR3/CFP at the SCV was lower. Whether this is the consequence of the altered interactions is unclear.

Figure 7. Interactions between HLA-DR3 and HLA-DM on Phagosomal Membranes.

(**A**) Salmonella containing vacuoles (SCV), MIIC and internal vesicles. HEK293 cells expressing DR3/CFP, DM/YFP and Ii were infected with *Salmonella* for 4 hr prior to fixation and processing for immuno-EM. Left panel shows two SCV that have considerably expanded (asterices). The SCV label for DR (15 nm gold) and DM (10 nm gold) at the limiting membrane, and lack internal structures. Inset: higher magnification of MIIC labeling for DR and DM within the same section. Right panel: formation of internal structures upon *Salmonella* death. The typical dense structures represent remnants of *Salmonella* in a structure labeling for DR and DM. Note the appearance of internal structures.

(**B**) Interactions between DO/CFP and DM/YFP on SCV. HEK293 cells expressing DO/CFP and DM/YFP were infected by mRFP expressing *Salmonella* for 4 hr before imaging by CLSM-FRET at 37°C. DO/CFP, DM/YFP and mRFP-*Salmonella* can be simultaneously detected, as indicated. The cell boundary and the nucleus are drawn in the image showing the location of the bacterium. The expanded SCV are detectable in the CFP and YFP channels. Donor FRET efficiency (E_D) is shown in false colors with the corresponding values. The efficiency of interaction between DO and DM is not affected on the *Salmonella*-containing vacuoles. Inset: magnification of the SCV region depicted in the E_D picture with a projection of *Salmonella* in pink (n > 50 observations).

(**C**) DR3/CFP and DM/YFP fail to interact in mRFP-expressing *Salmonella* containing vacuoles. HEK293 cells expressing DR3/CFP, DM/YFP and Ii were infected with mRFP-*Salmonella* for 4 hr before analysis by CLSM-FRET at 37°C. The various fluorophores were detected as in B. mRFP-*Salmonella* containing phagosomes with DR3/CFP and DM/YFP did not show FRET in contrast to normal MIIC in the same cell. (n > 60 observations). Note that a number of these normal MIIC are located close to the SCV.

(**D**) Analysis of FRET efficiency images. The images in (B) and (C) were analyzed as described in Figure 3E. The gray region depicts the threshold settings in these experiments. The CFP and YFP intensities of the pixels corresponding to the limiting membrane of the SCV, where no FRET was detected, are indicated in purple in the DO/CFP, DM/YFP (top), and the DR3/CFP and DM/YFP (bottom) plots. The intensities of DR3/CFP and DM/YFP on the SCV are comparable to MIIC within the same cell where normal FRET is measured.

(**E**) Peptide loading of DR3/CFP in subcellular fractions. HEK293 cells expressing DR3/CFP, DM/YFP, and Ii were infected with *Salmonella* for 4 hr, followed by subcellular fractionation (fraction 1–10). After fractionation, the vesicles were pelleted, incubated in SDS-loading buffer, and analyzed by SDS-PAGE and Westernblotting with various antibodies (bottom panel). The position of the various proteins is indicated. Fraction 5–6 showed β-hexosaminidase activity (top panel), and corresponded to MIIC. Fraction 6,7, marked by MHC class I, contained the plasma membrane (PM/ER). The SCV ran at a high density and contained a 30 kDa protein (fraction 9,10). Right lane: longer exposure of fraction 10. The conditions used, separated unstable (DRα, 35 kDa) from compact DR3/CFP molecules (DRαβ-CFP, 85 kDa). Compact DR/CFP molecules were located in the MIIC and PM/ER fractions, but were virtually absent in the SCV fractions.

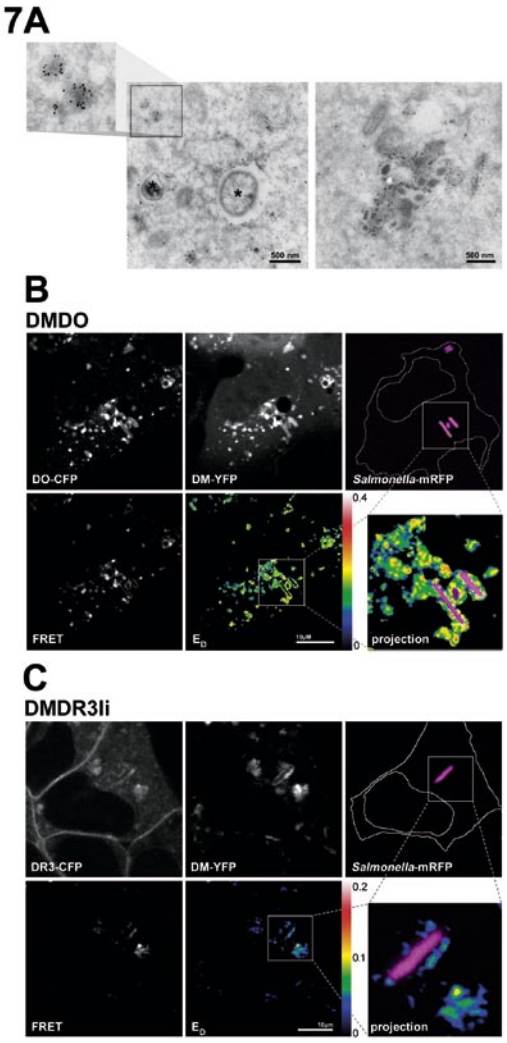

Still, the effect on DM/DR interactions is local. In the same cells, "normal" MIIC were found where DM and DR3 associated both in biochemical and FRET assays. Fractionation studies indicated that MHC class II loading occurs in MIIC structures but poorly in SCV. This suggests that intracellularly growing bacteria prevent local MHC class II presentation by preventing the formation of the typical architecture found in MIIC. At present, it is unclear whether this is just the result of their physical size or a situation actively maintained by the bacterium. In approximately 35% of the cases, we detected FRET between DM and DR3 in *Salmonella* containing phagosomes, which could be the result of death and disintegration of the bacterium; conditions where internal DM- and DR3-containing structures reappear in the SCV. However, surviving and viable intracellular pathogens will remain undetected by $CD4^+$ T cells as long as they prevent leakage of antigens into conventional MIIC. This local immune evasion may explain why other antigen presenting molecules have been developed, the CD1 family, to present antigens in a manner independent of DM (71).

We have visualized the interaction of DM and DR3 in living cells by FRET and have defined an MHC class II loading microdomain. DR3 interacted with its chaperone DM only on the internal membranes within an MIIC. Consequently, structures containing only a limiting membrane will not support efficient interactions between these two molecules, a situation observed in phagosomes. By preventing the formation of the conventional architecture of MIIC, *Salmonella* excludes the creation of MHC class II-loading microdomains, resulting in ineffective antigen presentation by MHC class II molecules.

Acknowledgments

We thank Eric Reits, Tom Groothuis, Joost Neijssen, and Ingrid Jordens for discussions, Lauran Oomen for help with CLSM images, Nico Ong for photography, and Adam Benham and Nicole van der Wel for reading the manuscript. This work was supported by grants from the Dutch Cancer Society KWF and the Netherlands Scientific Organization N.W.O.

References

1. Bryant, P.W., et al., Proteolysis and antigen presentation by MHC class II molecules. Adv Immunol, 2002. 80: p. 71-7114.
2. Peters, P.J., et al., Segregation of MHC class II molecules from MHC class I molecules in the Golgi complex for transport to lysosomal compartments. Nature, 1991. 349(6311): p. 669-676.
3. Cresswell, P., Chemistry and functional role of the invariant chain. Curr Opin Immunol, 1992. 4(1): p. 87-92.
4. Denzin, L.K. and P. Cresswell, HLA-DM induces CLIP dissociation from MHC class II alpha beta dimers and facilitates peptide loading. Cell, 1995. 82(1): p. 155-165.
5. Kropshofer, H., et al., HLA-DM acts as a molecular chaperone and rescues empty HLA-DR molecules at lysosomal pH. Immunity, 1997. 6(3): p. 293-302.
6. Sherman, M.A., D.A. Weber, and P.E. Jensen, DM enhances peptide binding to class II MHC by release of invariant chain-derived peptide. Immunity, 1995. 3(2): p. 197-205.
7. Chou, C.L. and S. Sadegh-Nasseri, HLA-DM recognizes the flexible conformation of major histocompatibility complex class II. J Exp Med, 2000. 192(12): p. 1697-1706.
8. Sanderson, F., et al., Association between HLA-DM and HLA-DR *in vivo*. Immunity, 1996. 4(1): p. 87-96.
9. Vogt, A.B., et al., Quality control of MHC class II associated peptides by HLA-DM/H2-M. Semin Immunol, 1999. 11(6): p. 391-403.
10. Doebele, R.C., et al., Determination of the HLA-DM interaction site on HLA-DR molecules. Immunity, 2000. 13(4): p. 517-527.
11. Pashine, A., et al., Interaction of HLA-DR with an acidic face of HLA-DM disrupts sequence-dependent interactions with peptides. Immunity, 2003. 19(2): p. 183-192.
12. Ullrich, H.J., et al., Interaction between HLA-DM and HLA-DR involves regions that undergo conformational changes at lysosomal pH. Proc Natl Acad Sci U S A, 1997. 94(24): p. 13163-13168.
13. Denzin, L.K., et al., Negative regulation by HLA-DO of MHC class II-restricted antigen processing. Science, 1997. 278(5335): p. 106-109.
14. Liljedahl, M., et al., Altered antigen presentation in mice lacking H2-O. Immunity, 1998. 8(2): p. 233-243.
15. van Ham, S.M., et al., HLA-DO is a negative modulator of HLA-DM-mediated MHC class II peptide loading. Curr Biol, 1997. 7(12): p. 950-957.
16. Calafat, J., et al., Major histocompatibility complex class II molecules induce the formation of endocytic MIIC-like structures. J Cell Biol, 1994. 126(4): p. 967-977.
17. Kleijmeer, M.J., et al., Major histocompatibility complex class II compartments in human and mouse B lymphoblasts represent conventional endocytic compartments. J Cell Biol, 1997. 139(3): p. 639-649.
18. Gruenberg, J., Lipids in endocytic membrane transport and sorting. Curr Opin Cell Biol, 2003. 15(4): p. 382-388.
19. Wubbolts, R., et al., Proteomic and biochemical analyses of human B cell-derived exosomes. Potential implications for their function and multivesicular body formation. J Biol Chem, 2003. 278(13): p. 10963-10972.
20. Escola, J.M., et al., Selective enrichment of tetraspan proteins on the internal vesicles of multivesicular endosomes and on exosomes secreted by human B-lymphocytes. J Biol Chem, 1998. 273(32): p. 20121-20127.
21. Hammond, C., et al., The tetraspan protein CD82 is a resident of MHC class II compartments where it associates with HLA-DR, -DM, and -DO molecules. J Immunol, 1998. 161(7): p. 3282-3291.
22. Kropshofer, H., et al., Tetraspan microdomains distinct from lipid rafts enrich select peptide-MHC class II complexes. Nat Immunol, 2002. 3(1): p. 61-68.
23. Katzmann, D.J., G. Odorizzi, and S.D. Emr, Receptor downregulation and multivesicular-body sorting. Nat Rev Mol Cell Biol, 2002. 3(12): p. 893-905.
24. Fernandez-Borja, M., et al., Multivesicular body morphogenesis requires phosphatidyl-inositol 3-kinase activity. Curr Biol, 1999. 9(1): p. 55-58.
25. Morrison, L.A., et al., Differences in antigen presentation to MHC class I-and class II-restricted influenza virus-specific cytolytic T lymphocyte clones. J Exp Med, 1986. 163(4): p. 903-921.
26. Song, W., et al., Wortmannin, a phosphatidylinositol 3-kinase inhibitor, blocks the assembly of peptide-MHC class II complexes. Int Immunol, 1997. 9(11): p. 1709-1722.
27. Brumell, J.H. and S. Grinstein, *Salmonella* redirects phagosomal maturation. Curr Opin Microbiol, 2004. 7(1): p. 78-84.
28. Russell, D.G., Phagosomes, fatty acids and tuberculosis. Nat Cell Biol, 2003. 5(9): p. 776-778.
29. Harding, C.V., L. Ramachandra, and M.J. Wick, Interaction of bacteria with antigen presenting cells: influences on antigen presentation and antibacterial immunity. Curr

Opin Immunol, 2003. 15(1): p. 112-119.
30. Ramachandra, L., et al., Processing of Mycobacterium tuberculosis antigen 85B involves intraphagosomal formation of peptide-major histocompatibility complex II complexes and is inhibited by live bacilli that decrease phagosome maturation. J Exp Med, 2001. 194(10): p. 1421-1432.
31. Ullrich, H.J., W.L. Beatty, and D.G. Russell, Interaction of *Mycobacterium avium*-containing phagosomes with the antigen presentation pathway. J Immunol, 2000. 165(11): p. 6073-6080.
32. Vergne, I., J. Chua, and V. Deretic, Tuberculosis toxin blocking phagosome maturation inhibits a novel Ca2+/calmodulin-PI3K hVPS34 cascade. J Exp Med, 2003. 198(4): p. 653-659.
33. Hernandez, L.D., et al., *Salmonella* modulates vesicular traffic by altering phosphoinositide metabolism. Science, 2004. 304(5678): p. 1805-1807.
34. Stam, N.J., H. Spits, and H.L. Ploegh, Monoclonal antibodies raised against denatured HLA-B locus heavy chains permit biochemical characterization of certain HLA-C locus products. J Immunol, 1986. 137(7): p. 2299-2306.
35. Vennegoor, C. and P. Rumke, Circulating melanoma-associated antigen detected by monoclonal antibody NKI/C-3. Cancer Immunol Immunother, 1986. 23(2): p. 93-100.
36. Adams, T.E., J.G. Bodmer, and W.F. Bodmer, Production and characterization of monoclonal antibodies recognizing the alpha-chain subunits of human ia alloantigens. Immunology, 1983. 50(4): p. 613-24.
37. Shaw, S., A. Ziegler, and R. DeMars, Specificity of monoclonal antibodies directed against human and murine class II histocompatibility antigens as analyzed by binding to HLA-deletion mutant cell lines. Hum Immunol, 1985. 12(4): p. 191-211.
38. Neefjes, J.J., et al., The biosynthetic pathway of MHC class II but not class I molecules intersects the endocytic route. Cell, 1990. 61(1): p. 171-83.
39. van Ham, S.M., et al., HLA-DO is a negative modulator of HLA-DM-mediated MHC class II peptide loading. Curr Biol, 1997. 7(12): p. 950-7.
40. Morton, P.A., et al., Delivery of nascent MHC class II-invariant chain complexes to lysosomal compartments and proteolysis of invariant chain by cysteine proteases precedes peptide binding in B-lymphoblastoid cells. J Immunol, 1995. 154(1): p. 137-50.
41. Copier, J., et al., Targeting signal and subcellular compartments involved in the intracellular trafficking of HLA-DMB. J Immunol, 1996. 157(3): p. 1017-27.
42. van Ham, M., et al., Modulation of the major histocompatibility complex class II-associated peptide repertoire by human histocompatibility leukocyte antigen (HLA)-DO. J Exp Med, 2000. 191(7): p. 1127-36.
43. Marks, M.S., et al., A lysosomal targeting signal in the cytoplasmic tail of the beta chain directs HLA-DM to MHC class II compartments. J Cell Biol, 1995. 131(2): p. 351-69.
44. Nijenhuis, M., et al., Targeting major histocompatibility complex class II molecules to the cell surface by invariant chain allows antigen presentation upon recycling. Eur J Immunol, 1994. 24(4): p. 873-83.
45. Kanda, T., K.F. Sullivan, and G.M. Wahl, Histone-GFP fusion protein enables sensitive analysis of chromosome dynamics in living mammalian cells. Curr Biol, 1998. 8(7): p. 377-85.
46. Brummelkamp, T.R., R. Bernards, and R. Agami, A system for stable expression of short interfering RNAs in mammalian cells. Science, 2002. 296(5567): p. 550-3.
47. Van Rheenen, J., M. Langeslag, and K. Jalink, Correcting confocal acquisition to optimize imaging of fluorescence resonance energy transfer by sensitized emission. Biophys J, 2004. 86(4): p. 2517-29.
48. Vermeer, J.E., et al., Probing plasma membrane microdomains in cowpea protoplasts using lipidated GFP-fusion proteins and multimode FRET microscopy. J Microsc, 2004. 214(Pt 2): p. 190-200.
49. Boes, M., et al., T-cell engagement of dendritic cells rapidly rearranges MHC class II transport. Nature, 2002. 418(6901): p. 983-988.
50. Wubbolts, R., et al., Direct vesicular transport of MHC class II molecules from lysosomal structures to the cell surface. J Cell Biol, 1996. 135(3): p. 611-622.
51. Marks, M.S., et al., A lysosomal targeting signal in the cytoplasmic tail of the beta chain directs HLA-DM to MHC class II compartments. J Cell Biol, 1995. 131(2): p. 351-369.
52. Germain, R.N. and L.R. Hendrix, MHC class II structure, occupancy and surface expression determined by post-endoplasmic reticulum antigen binding. Nature, 1991. 353(6340): p. 134-139.
53. Neefjes, J.J. and H.L. Ploegh, Inhibition of endosomal proteolytic activity by leupeptin blocks surface expression of MHC class II molecules and their conversion to SDS resistance alpha beta heterodimers in endosomes. EMBO J, 1992. 11(2): p. 411-416.
54. Förster, T., Zwischenmolekulare Energiewandering und Fluoreszenz. . Annalen Physik, 1948. 6: p. 55-75.
55. Tsien, R.Y., The green fluorescent protein. Annu Rev Biochem, 1998. 67: p. 509-544.
56. Ormo, M., et al., Crystal structure of the *Aequorea victoria* green fluorescent protein. Science, 1996. 273(5280): p. 1392-1395.
57. Mosyak, L., D.M. Zaller, and D.C. Wiley, The structure of HLA-DM, the peptide exchange catalyst that loads antigen onto class II MHC molecules during antigen presentation. Immunity, 1998.

9(3): p. 377-383.
58. Ghosh, P., et al., The structure of an intermediate in class II MHC maturation: CLIP bound to HLA-DR3. Nature, 1995. 378(6556): p. 457-462.
59. van Rheenen, J., M. Langeslag, and K. Jalink, Correcting confocal acquisition to optimize imaging of fluorescence resonance energy transfer by sensitized emission. Biophys J, 2004. 86(4): p. 2517-2529.
60. van Lith, M., et al., Regulation of MHC class II antigen presentation by sorting of recycling HLA-DM/DO and class II within the multivesicular body. J Immunol, 2001. 167(2): p. 884-892.
61. Bastiaens, P.I. and A. Squire, Fluorescence lifetime imaging microscopy: spatial resolution of biochemical processes in the cell. Trends Cell Biol, 1999. 9(2): p. 48-52.
62. Vermeer, J.E.M., et al., Probing plasma membrane microdomains in cowpea protoplasts using lipidated GFP-fusion proteins and multimode FRET microscopy. J Microsc, 2004. 214(Pt 2): p. 190-200.
63. van Ham, M., et al., Modulation of the major histocompatibility complex class II-associated peptide repertoire by human histocompatibility leukocyte antigen (HLA)-DO. J Exp Med, 2000. 191(7): p. 1127-1136.
64. Ohkuma, S. and B. Poole, Cytoplasmic vacuolation of mouse peritoneal macrophages and the uptake into lysosomes of weakly basic substances. J Cell Biol, 1981. 90(3): p. 656-664.
65. Allen, P.M. and E.R. Unanue, Antigen processing and presentation by macrophages. Am J Anat, 1984. 170(3): p. 483-490.
66. Honey, K. and A.Y. Rudensky, Lysosomal cysteine proteases regulate antigen presentation. Nat Rev Immunol, 2003. 3(6): p. 472-482.
67. Sanderson, F., et al., Accumulation of HLA-DM, a regulator of antigen presentation, in MHC class II compartments. Science, 1994. 266(5190): p. 1566-1569.
68. Zur Lage, S., et al., Activation of macrophages and interference with CD4+ T-cell stimulation by Mycobacterium avium subspecies paratuberculosis and *Mycobacterium avium* subspecies avium. Immunology, 2003. 108(1): p. 62-69.
69. Flynn, J.L. and J. Chan, Immune evasion by *Mycobacterium tuberculosis*: living with the enemy. Curr Opin Immunol, 2003. 15(4): p. 450-455.
70. Beuzon, C.R., et al., pH-dependent secretion of SseB, a product of the SPI-2 type III secretion system of *Salmonella typhimurium*. Mol Microbiol, 1999. 33(4): p. 806-816.
71. Vincent, M.S., J.E. Gumperz, and M.B. Brenner, Understanding the function of CD1-restricted T cells. Nat Immunol, 2003. 4(6): p. 517-523.

Supplemental Figures

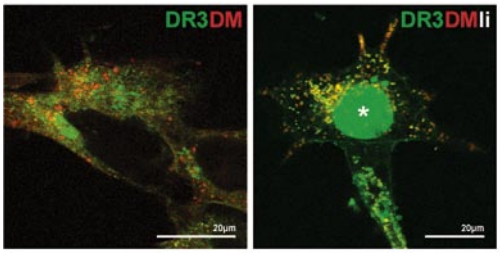

Figure S1. The invariant chain Ii releases HLA-DR/CFP from the ER for transport to HLA-DM containing MIIC and the plasma membrane. HEK293 cells stably expressing DR3/CFP and DM/YFP (left panel) were microinjected with expression vectors for Ii and H2B-GFP (asterix). The position of DR3 (in green) and DM (in red) was subsequently monitored. In the absence of Ii, DR3/CFP is strongly expressed in the ER. Ii induces ER release and transport to DM containing vesicles and the plasma membrane.

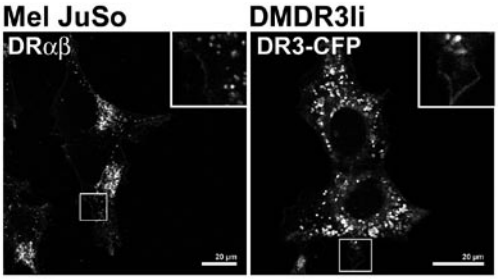

Figure S2. HLA-DR3/CFP has a similar intracellular distribution compared to HLA-DR3 expressed endogenously. Mel JuSo cells endogenously expressing DR were fixed with methanol and stained with anti-DRαβ antibody (left panel). Both intracellular distribution and cell surface expression of DR is comparable to that of DR3/CFP in the HEK293 transfectant also expressing DM/YFP and Ii (right panel). Inset shows a zoom-in of the surface expression.

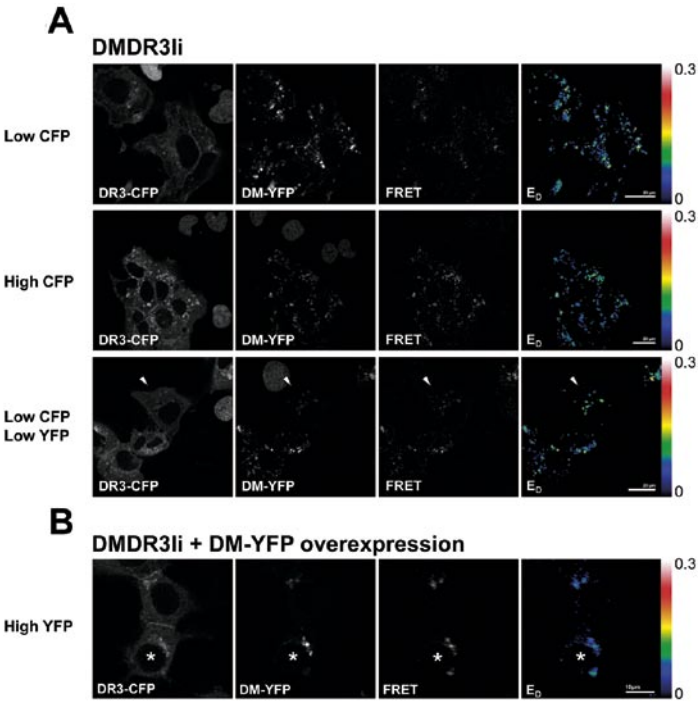

Figure S3. MIIC of HEK293 cells expressing different ratios of HLA-DR/CFP versus HLA-DM/YFP show similar donor FRET efficiencies.
(**A**) The interaction between DR3/CFP and DM/YFP was measured by confocal-FRET on stable HEK293 transfectants at 37°C. Cells with different levels of DR/CFP were selected as indicated. The CFP signal, YFP signal, FRET and donor FRET efficiency (E_D) measurements are depicted (details in Fig 3A). FRET efficiency between DR3/CFP and DM/YFP is not affected by varying levels of donor DR3/CFP molecules, suggesting saturating amounts of DM/YFP in these vesicles.
(**B**) The interaction between DR3/CFP and DM/YFP was measured by confocal-FRET on stable HEK293 transfectants transiently over-expressing DM/YFP (marked with an asterix). The CFP signal, YFP signal, FRET and donor FRET efficiency (E_D) measurements are depicted. FRET efficiency between DR3/CFP and DM/YFP is not altered by the increasing levels of acceptor DM/YFP molecules.

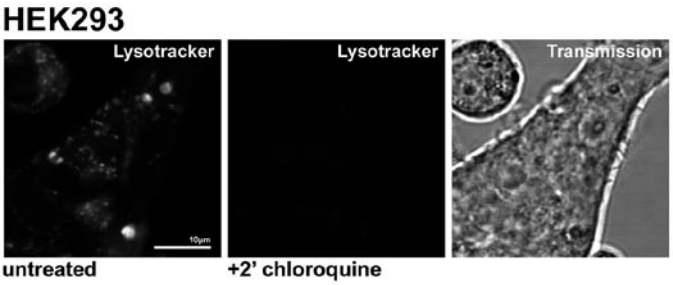

Figure S4. 2' chloroquine treatment suffices to neutralize MIIC. Living HEK293 cells were incubated at 37°C with Lysotracker-Red to visualize acidic vesicles, including MIIC (Left panel). This fluorescence was lost within 2 min after addition of 100µM chloroquine (Middle panel). Right panel, transmission image of the assayed cell.

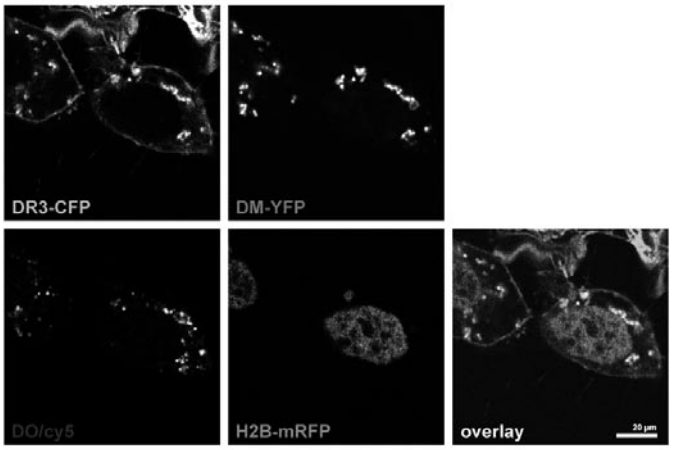

Figure S5. HLA-DO overexpression in fixed cells. HEK293 cells stably expressing DR3/CFP and DM/YFP, and over-expressing unlabeled DO and H2B-mRFP as an transfection marker, were fixed with formaldehyde and stained with anti-DOβ antibody (42). Cells expressing nuclear mRFP also contain DO, which colocalizes with DM/YFP and DR/CFP in perinuclear vesicles.

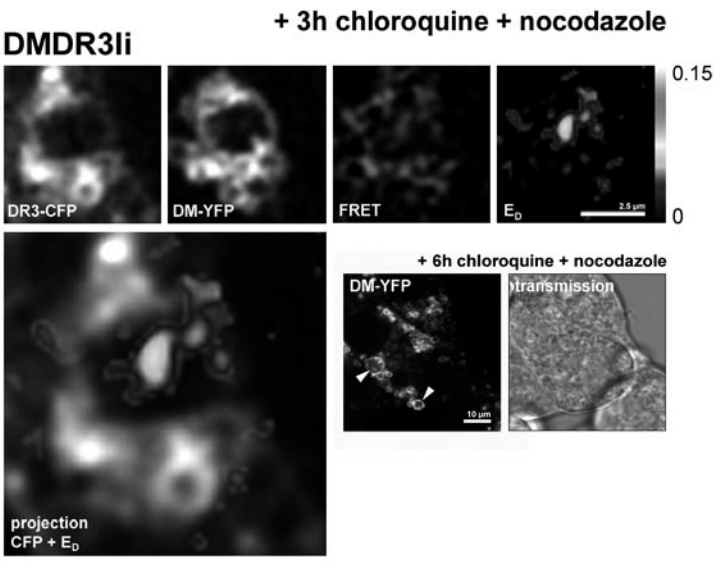

Figure S6. Vesicle transport is not required for chloroquine-induced expansion of MIIC. HEK293 cells expressing DR/CFP, DM/YFP and Ii were treated with nocodazole to disrupt the microtubulular network, and block vesicular transport. Subsequently, the cells were cultured in the presence of 100µM chloroquine, and FRET was measured between DR3/CFP and DM/YFP on the expanded structures (shown is a zoom-in of the expanded structure). No efficient FRET was detected on the limiting membrane of the (expanded) MIIC. The subpanel shows the location of DM/YFP after 6 h culture in the presence of chloroquine and nocodazole. MIIC completely expanded in the absence of microtubule-based vesicle transport, which suggests that the lipids required for the expanded limiting membrane almost exclusively derive from internal vesicles. Note that long-term treatment with nocodazole altered the morphology of the cells.

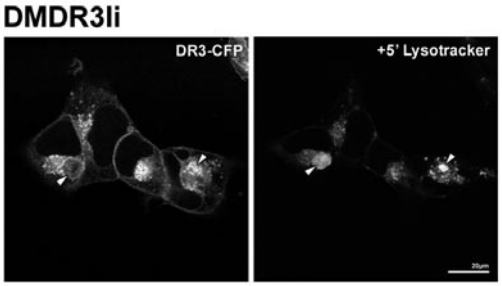

Figure S7. Swollen MIICs induced by knockdown of VPS34 remain acidic. HEK293 cells expressing DR/CFP, DM/YFP and Ii were transfected with an RNAi construct for hVPS34. Imaging 72 h after transfection revealed swollen DR/CFP containing vesicles (indicated by arrows in left panel). These vesicles accumulated Lysotracker-Red (right panel), indicating that they were acidic.

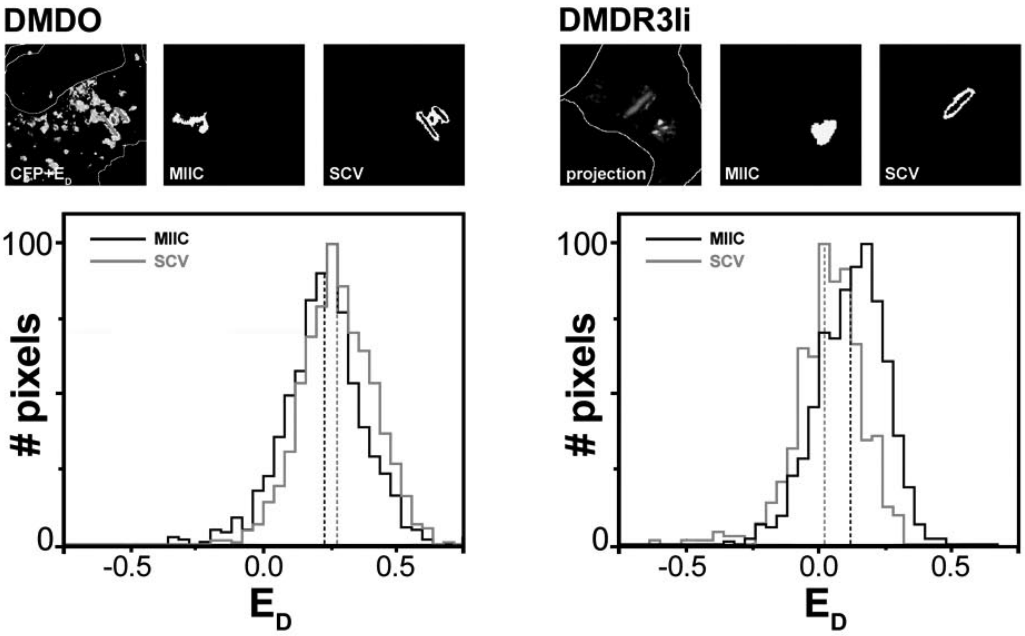

Figure S8. Donor FRET efficiency distribution of pixels representing SCV and MIIC. The data shown in Figure 7 were analyzed for donor FRET efficiency (E_D) distribution. MIIC or SCV pixels from the cells expressing DO/CFP, DM/YFP, or DR3/CFP, DM/YFP and Ii were extracted as shown in the top panel. The distribution of the donor FRET efficiencies of these selected pixels were plotted in a histogram (bottom panel). The average values are indicated by the dotted lines. Note the Poisson distribution of the E_D values, which is a consequence of noise in the measurements. Whereas E_D distribution for DO/CFP and DM/YFP is identical on both MIIC and SCV, a clear difference is observed for DR3/CFP and DM/YFP. No interaction between DR3 and DM is observed at the SCV.

Supplemental Information On FRET Calculations

For further details, see van Rheenen et al. Biophys J. 2004 vol. 86, pp.2517-2529.

FRET between CFP and YFP can be studied by calculating the sensitized emission (F_{Sen}), the acceptor emission upon donor excitation, from separately acquired CFP and YFP images. CFP and YFP have a spectral overlap. Therefore, the detected sensitized emission must be corrected for CFP leak-through into the acceptor channel and direct excitation of YFP during CFP excitation to obtain the measured sensitized emission (M_{Sen}). Consequently, three images were acquired, M_{CFP}; CFP excitation and CFP detection, $M_{IndirectYFP}$; CFP excitation and YFP detection, $M_{DirectYFP}$; YFP excitation and YFP detection. From the $M_{IndirectYFP}$ image, sensitized emission was calculated using the following equation:

$$M_{Sen} = (M_{IndirectYFP} - \beta M_{CFP} - (\gamma - \alpha\beta) M_{DirectYFP} \text{ image}) / (1 - \beta\delta),$$

where α is the correction factor for YFP fluorescence excited and detected at CFP wavelength, β the leakthrough factor of fluorescence of CFP into YFP filters, δ the leakthrough factor of sensitized emission back onto the CFP filters, and γ the excitation efficiency of the YFP upon CFP excitation. These correction factors were obtained by co-culturing the cells of interest with cells expressing CFP and YFP only.

α, γ, δ are obtained by imaging a cell containing only YFP and calculated as:

$$\alpha = M_{CFP}/M_{DirectYFP}$$

$$\gamma = M_{IndirectYFP}/M_{DirectYFP}$$

$$\delta = M_{CFP}/M_{IndirectYFP}$$

β is obtained by imaging a cell containing CFP only and calculated as:

$$\beta = M_{IndirectYFP}/M_{CFP}$$

To obtain the efficiency of FRET, CFP fluorescence lost by FRET and measured in the M_{CFP} channel ($Lost_{CFP}$) is related by the total CFP fluorescence measured in the M_{CFP} channel (CFP fluorescence when FRET equals zero, $Total_{CFP}$) as:

$$E_D = Lost_{Sen}/Total_{CFP},$$

where $Lost_{CFP}$ relates to the sensitized emission measured in the $M_{IndirectYFP}$ channel (M_{sen}) as

$$Lost_{CFP} = (Q_{CFP}/Q_{YFP})(C/(\beta\Delta))M_{sen},$$

and the total CFP fluorescence as:

$$Total_{CFP} = (1+\zeta)M_{CFP} - (\zeta/\beta)M_{IndirectYFP} - (\alpha - \zeta((\gamma - \alpha\beta)/\beta))M_{DirectYFP},$$

where Q_{CFP} and Q_{YFP} are the quantum yield of respectively CFP and YFP, C is the fraction of CFP spectrum in the YFP channel, D the fraction of YFP spectrum in the YFP channel and ζ is a constant which can be derived from

$$\zeta = (\delta\beta - ((CQ_{CFP}/DQ_{YFP})/(1-\beta\delta))).$$

To reliably calculate sensitized emission, corrections should be performed on major sources of error and variability in confocal acquisition of M_{CFP}, $M_{IndirectYFP}$ and $M_{DirectYFP}$ images. Since different laser lines are used to excite CFP and YFP (430nm for M_{CFP} and $M_{IndirectYFP}$ and 514 nm for $M_{DirectYFP}$), chromatic aberrations within the objective and other optics, and small collimation differences in the laser beams result in an axial offset in the optical section of the acquired CFP and YFP images. To correct for this, M_{CFP} and $M_{IndirectYFP}$ images were acquired using 430nm excitation (optimal excitation for measuring FRET). Then, using the Z-galvanometer of the microscope stage, the preparation is refocused to minimize the axial offset where after the $M_{DirectYFP}$ image is acquired using 514nm excitation. After image acquisition, images were corrected for lateral image errors. The excitation intensity varies within an image (most apparent at the borders of an image), especially in confocal acquisition since the different excitation sources give different excitation intensity distributions. Because these excitation inhomogeneities are constant over time, they were corrected by normalizing the acquired images by reference images (e.g. images of CFP and YFP solutions). The excitation intensity not only varies laterally, but temporally as well, which makes the calculation of sensitized emission extremely difficult, since the correction factors α and γ will change in time. To correct for this, for every pair of images acquired, new control cells were imaged to reliably recalculate the correction factors. For exact details, see van Rheenen and co-workers (2004).